



Nanophotonic waveguides for biomolecular transport and particle control

by Allen Yang

This thesis/dissertation document has been electronically approved by the following individuals:

Stroock, Abraham Duncan (Chairperson)

Shuler, Michael Louis (Minor Member)

Erickson, David (Minor Member)

Lipson, Michal (Additional Member)

NANOPHOTONIC WAVEGUIDES FOR BIOMOLECULAR TRANSPORT AND
PARTICLE CONTROL

A Dissertation

Presented to the Faculty of the Graduate School
of Cornell University

In Partial Fulfillment of the Requirements for the Degree of
Doctor of Philosophy

by

Allen Yang

August 2010

© 2010 Allen Yang

NANOPHOTONIC WAVEGUIDES FOR BIOMOLECULAR TRANSPORT AND PARTICLE CONTROL

Allen Yang, Ph. D.

Cornell University 2010

Current separation and fractionation technologies developed for lab-on-a-chip platforms are often unable to differentiate single particles or objects from those with similar properties (eg. size or charge). One potential solution to this dilemma uses focused optical fields for remote and precise control of discrete microscale objects. While optical tweezers and similar technologies are useful tools for microparticle or cellular manipulation, these methods are fundamentally limited by light diffraction. The consequences of these limitations are: (1) it is extremely difficult to optically manipulate nanoscale (below 100 nm in size) particles and (2) movement of trapped particles are generally restricted to two dimensions. Previous work by the author (Master's thesis) has shown that optical waveguides integrated into microfluidic channels can use the evanescent field to trap and manipulate particles using gradient and radiation pressure forces.

This dissertation extends the previous work and focuses on methods for nanoparticle trapping by using nanophotonic devices which can exert greater optical forces. Slotted waveguides confine light within a nanoscale slot cut into a silicon waveguide that provides access to more optical energy and increases the strength of the optical trapping force. Microring resonators use an optical resonance effect to amplify the

optical field within the ring structure which can be used to exert precise control over trapped particles. This study contains the following key results: (1) controlled trapping and release of dielectric nanoparticles and single biomolecules in silicon slot waveguides, (2) a comprehensive analytical and numerical study of particle trapping on nanometer length scales in slot waveguides, and the (3) integration of microring resonators and microfluidics to enable optically controlled switched for particles trapped on waveguides.

The nanophotonic architectures for optofluidic transport demonstrated in this work can be integrated into lab-on-a-chip platforms using existing manufacturing techniques. They allow for the discrete optical manipulation and transport of nanoscopic objects with greater precision and control than is available with existing approaches. Future potential applications include integrated sensor/trapping capabilities for lab-on-a-chip devices and sophisticated particle manipulation in microfluidic environments. This fusion of nanofluidics and optical manipulation could lead to new methods for biomedical diagnostics and biochemical processing.

BIOGRAPHICAL SKETCH

Allen Yang is currently a graduate student in the School of Chemical and Biomolecular Engineering at Cornell University since 2005. His work is conducted in the Integrated Micro- and Nanofluidic Systems laboratory under Prof. David Erickson. Allen received his B.S. in chemical engineering with minors in biomedical engineering and colloids, polymers, and surfaces from Carnegie Mellon University in 2005. In the summer of 2004, he participated in the NNIN REU program at Cornell University under the direction of Prof. Abraham Stroock investigating the self-assembly of shaped colloidal structures. Previously, he graduated from Montville Township High School in Montville, NJ in 2001. His current research interests involve developing lab-on-a-chip devices for biomedical diagnostics and biochemical processing.

For my mom and dad, for all their love and support

ACKNOWLEDGMENTS

I'd first like to thank David Erickson, my advisor, for the guidance and support that I have received so far during my time as a grad student. He has taught me a lot about working as an academic and let me be involved in the research process on many levels. There is no one I consider a more dedicated scientist and teacher than he has proven to be.

I also would like to thank Abraham Stroock and Susan Daniel, who have been two very good mentors to me. Abe introduced me to the world of microscale and nanoscale research and since working with him, I have never looked back. He has also been an invaluable mentor and role model for me. When I began as a TA for Susan, I never imagined all the things that we would accomplish in that one semester. Thanks to her I have gained a ton of experience in teaching, lecturing, and in developing course material. I also appreciate her friendship and support through this last year and as a sounding board as I tried to decide on my post-grad career.

I would like to thank my labmates and fellow grad students for the camaraderie and friendship I have received over the last 5 years, it has been a fun and wonderful time. In particular, I'd like to thank Brad Schmidt, Art Nitkowski from the Lipson group for discussions and just knowing everything there is to know about optics. I'd also like to thank Roman Akhmechet and Henry Lau, the 'silent duo', who were there for support when things went awry and kept me laughing in the bad times.

Finally, I'd like to thank my family and friends for their support. My parents, David and Wendy, keep me grounded and remind me that there is life outside grad school. Alex, my brother, reminds me by showing me his new car. Thanks to all of you for putting up with me and being there for me.

This work was partially supported by the following:

NSF Grant CBET-0529045- "Integration of spectroscopic sensors and electroactive nanowell arrays with microfluidic chips based on thermocapillary actuation"

NSF NIRT Grant CBET- 0708599- “Active Nanophotofluidic Systems for Single Molecule/Particle Analysis”

Cornell NanoScale Facility- A member of the National Nanotechnology Infrastructure Network, which is supported by the National Science Foundation (Grant ECS 03-35765).

TABLE OF CONTENTS

BIOGRAPHICAL SKETCH.....	III
DEDICATION	IV
ACKNOWLEDGMENTS	V
TABLE OF CONTENTS	VII
LIST OF FIGURES	IX
LIST OF TABLES	X
1.0 INTRODUCTION	1
1.1 TRANSPORT IN MICROFLUIDIC DEVICES	2
1.2 OPTICAL MANIPULATION IN MICROFLUIDIC DEVICES	5
1.3 NEAR-FIELD AND EVANESCENT FIELD OPTICAL MANIPULATION	8
1.4 THEORY OF OPTOFLUIDIC TRANSPORT	12
1.4.1 <i>Hydrodynamic forces on a particle in a flow</i>	15
1.4.2 <i>Solution of wave equation for dielectric slab waveguide</i>	16
1.4.3 <i>Electromagnetic forces on a particle</i>	18
1.4.5 <i>Optofluidic transport for non-Rayleigh particles</i>	21
2.0 OPTICAL MANIPULATION OF NANOPARTICLES AND BIOMOLECULES IN SUB-WAVELENGTH SLOT WAVEGUIDES.....	30
2.1 METHOD SUMMARY.....	41
2.2 SUPPLEMENTAL MATERIAL: KINETIC ANALYSIS OF TRAPPING STABILITY	42
3.0 FORCES AND TRANSPORT VELOCITIES FOR A PARTICLE IN A SLOTTED WAVEGUIDE.....	48
3.1 INTRODUCTION	48
3.2 RESULTS AND DISCUSSION	58
4.0 OPTOFLUIDIC RING RESONATOR SWITCH FOR OPTICAL PARTICLE TRANSPORT	72
4.1 INTRODUCTION	72
4.2 RESULTS AND DISCUSSION	74
4.2.1 <i>Particle switching using microring resonators</i>	76
4.3 DEVICE CHARACTERIZATION	78

4.4	MATERIALS AND METHODS.....	86
4.5	CONCLUSIONS.....	88
5.0	FUTURE WORK AND CONCLUSIONS.....	92
5.1	FUTURE WORK	92
5.2	SUMMARY AND CONCLUSION	96

LIST OF FIGURES

Figure 1.1: Forces on a particle trapped on a waveguide	22
Figure 2.1: Nanoscale optofluidic transport	32
Figure 2.2: Trapping and transport of dielectric nanoparticles in a slot waveguide	34
Figure 2.3: Capture and trapping of λ -DNA.....	35
Figure 2.4: Trapping forces on particles trapped inside and outside the slot waveguide, and analysis of particle release kinetics.....	37
Figure 3.1: Nanophotonic Optofluidic Transport	51
Figure 3.2: Comparison of Maxwell Stress Tensor (MST) to Rayleigh scattering	57
Figure 3.3: Trapping forces on nanoparticles in a 100 nm slot	60
Figure 3.4: Propulsion forces on nanoparticles in a 100 nm slot	62
Figure 3.5: Trapping force for nanoparticles in a 30 nm slot.....	65
Figure 4.1: Schematic of optofluidic ring resonator switch.	75
Figure 4.2: Active optical switching of particles on a microring resonator.	77
Figure 4.3: Optical transmission spectra of ring resonators and laser output	79
Figure 4.4: Enhancement of propulsion velocity	82
Figure 4.5: Particle switch efficiency as a function of input wavelength.....	84

LIST OF TABLES

Table 3.1: Simulation and Geometric Parameters	53
Table 3.2: Stability, trapping stiffness , and steady state velocities	67

1.0 Introduction

In recent years, there has been an increased need for discrete and remote handling of fluid samples in lab-on-a-chip devices. Optofluidics, which seeks to unite optical and fluid handling functions for mutual benefit, provides an unique opportunity for innovation. To illustrate, the state of the art in chip-based particle handling technology uses optical tweezers, or variants thereof, to provide the driving force behind optically driven manipulation. Integration with microfluidic environments has enabled sorting and fractionation processes for microscopic biological or synthetic particles. The fundamental limitation in free space trapping is the inability to generate the required forces for the manipulation of small objects over long interaction distances. High numerical aperture lenses are used to create intense optical spots, but greatly limit the focal length of the beam. Previous work by the author and others in the field have shown that the evanescent field of a waveguide structure can generate similar trapping forces, and can be integrated with microfluidics to create a new paradigm of optically-driven particle transport. Nanophotonic devices such as slotted waveguides and microring resonators provide a foundation of advanced optical devices that can control light in unique ways that can be exploited for transport purposes as well.

This dissertation presents the recent research methods, experiments, and analysis in the demonstrating the integration of advanced nanophotonic devices for the optofluidic manipulation of nanoparticles and biomolecules. This study has several improvements over previous works which include (1) controlled trapping and release of dielectric nanoparticles and single biomolecules in slot waveguides, (2) a comprehensive analytical and numerical study of particle trapping on nanometer length scales in slot waveguides, and the (3) integration of microring resonators and

microfluidics to enable optically controlled switched for particles trapped on waveguides.

Chapter 1 introduces the concept of optofluidics and discusses recent advances in optical manipulation in microfluidic devices. In addition, a summary of the fundamental phenomena and theory developed to understand optofluidic transport are covered. Chapter 2 details the results of experiments in trapping nanoparticles and DNA molecules in slot waveguides. Chapter 3 discusses the analytical and numerical study of particle trapping stability in slot waveguides and the limits of optofluidic transport within such an architecture. Chapter 4 covers the fabrication, demonstration, and characterization of an optofluidic transport switch for trapped particles based on a ring resonator architecture. Chapter 5 concludes the dissertation and discusses possible extensions of this work in the future.

1.1 Transport in Microfluidic Devices

Microfluidics is the study of flow behavior with micron scale confinement. In these systems, the amount of fluid manipulated is very small, ranging from microliters down to picoliters. This phenomena can be observed readily in nature, particularly in cardiovascular systems [1] and plant vascular systems [2]. In terms of fluid mechanics, these flows generally have very low Reynolds and Péclet numbers, which is characteristic of diffusive, laminar flow.

The dominant platform for microfluidically enabled devices comes in the form of lab-on-a-chip [3], sometimes known as a Micro-Total-Analysis-System [4] (μ TAS). These devices contain components for fluid handling [5], chemical processing [6], and sensing and analysis [7]. The complexity can range from a simple microchannel devices [8] to highly complex chips capable of handling all of the aforementioned

processes with little outside interaction. Part of the success of such technology is attributed to research into methods for conducting the same unit operations used in large-scale chemical processing on the microscale. Adaptations of this technology have enabled unit operations such as mixing [9], reactions [10], and separations [11] to be conducted in many ways on lab-on-a-chip devices. In addition, many novel methods for fluid manipulation allow for the batch processing of droplets of fluid [12], and the manipulation of fluid flow using electrokinetics [13-15].

The ability to conduct complex chemical processing has numerous advantages for future technologies, particularly in the realm of biochemical processing and microscale energy production. Key improvements that can be achieved by device miniaturization include: (1) cheap mass production costs, allowing for disposable chips, (2) lower operating costs due to small internal volumes (useful for rare or costly samples and reagents), and (3) high levels of integration along with the potential for multiplexed parallel processing. For these reasons, such devices have become useful for point of care testing [13] and miniaturized bioassays [14].

On length scales relevant to transport in micro- and nanofluidic devices, fluid flow and species transport can be accomplished by a number of elegant techniques, a few of which include: pressure driven flow [15], electrokinetics [16-19], buoyancy [20], magnetohydrodynamics [21], capillarity, electrowetting [22] and thermocapillarity [23]. There are a number of excellent references and textbooks that review different mechanisms of microfluidic transport [19, 24, 25]. In general, pressure driven and electrokinetics are most commonly employed of these varying methods, because of the low learning curve for implementation. Pressure driven flow is the most versatile, requiring only a pressure or vacuum source to generate flow while being compatible with almost any fluid and surface chemistries. On-chip valving techniques such as

multilayer soft-lithography [15] enable complex flow control and sample routing down to the scale of about 1 μm . However, as the velocity of a pressure driven flow scales proportionally with the square of the critical length of the channel, manipulating flows on such length scales proves impractical. Another limitation of pressure driven transport is velocity differential between the flow near the walls and the center of the channel. This causes an effect known as dispersion [26] which is undesirable in many separation and many mass transport applications.

Electrokinetic transport is flow that can be induced in a microchannel through the interactions of the fluid to an applied electric field. More specifically, fluid movement that is the result of the flow of charged ions near a channel wall due to the electric double layer effect is known as electroosmosis and the mass flow of charged particles in an applied DC field is known as electrophoresis. These mechanisms for fluid and mass flow exhibit a more favorable scaling ratio to channel dimensions as compared to pressure driven flow. On length scales greater than the limit where two electrical double layers overlap, the speed of electrokinetic transport is largely independent of channel height. Within the double layer overlapped regime the velocity scales approximately with $1-1/\kappa d$ [16], where $1/\kappa$ is the double layer thickness and d is the channel half-height. When κd is on the order of 1, which is likely in highly confined nanofluidic systems, the flow can be nearly entirely impeded. In practice, electrokinetic flow techniques are limited in the number of surface and fluid chemistries allowed. Fluids are often limited to aqueous solutions with low ionic concentration and surface conditions can result in extreme changes in flow properties. Furthermore, the exclusion of metallic and semiconductor substrates because of their electric conductance properties means that integration with other technologies is limited as well. The flow of charge through the channel can also result in significant

joule heating [27] leading to non-uniform viscosity fields and catastrophic boiling in polymeric substrates.

1.2 Optical Manipulation in Microfluidic Devices

While microfluidic flows could be altered using pressure gradients and electric fields, localized manipulation on sub-micron length scales requires a more precise approach. Optical trapping using focused laser beams was first pioneered by Arthur Ashkin in 1970 [28]. Over the next 20 years, many applications using optical tweezers to manipulate microscale objects have appeared. Some prominent examples include the trapping of bacteria cells and viruses [29] and metallic particles [30]. Stephen Chu pioneered the efforts in the laser cooling of single atoms using a three-axis radiation pressure driven trap [31]. Optical traps have also been used to study the hydrodynamic stretching of DNA molecules [32] by using microscopic beads with macromolecules attached. The beads are optically trapped, while the DNA or polymer is stretched via hydrodynamic forces. These studies laid the foundation for a breadth of work that focused on using optically derived forces within microfluidic devices for targeted applications.

The term “Optofluidics” [33, 34] has been used to collectively describe technology which has combined microfluidic and optical devices, generally in on-chip fabricated systems. Optofluidics can be further characterized into two different classes: (1) devices where microfluidics adds functionality to optical devices and (2) devices where optical elements add functions to microfluidic chips. In general, the first class of applications generally focuses on using microfluidic elements to enable changes to the local refractive index of photonic devices such as waveguides [35] and photonic crystals [36]. This is most often accomplished by overlaying fluidic channels over photonic systems and pumping fluids of different refractive index. The advantage of

integrating microfluidics in these systems is in multiplexed addressing of devices, and the insertion of line defects into photonic crystal structures.

Recently, researchers have been exploring the uses of light-based manipulation in integrated microfluidic devices. Current applications focus on particle concentration [37], sorting [38], and chromatography [39]. Unlike the traditional transport techniques described above, the main advantage of these optical approaches lies in their ability to handle individual particles directly, as opposed to indirect manipulation of the surrounding flow field. These mechanisms rely upon separations using properties such as size, refractive index, and absorption of light. Applications using such an approach incorporate traditional optical tweezing [14], rotational manipulation of components based on form birefringence, [19] and more recently developed electro-optic approaches such as that by Chiou *et al.* [20]. Applegate *et al.* [40] demonstrated the use diode laser bars as a method for active sorting in microfluidic channels. A more passive mechanism for size-based optical sorting was demonstrated by MacDonald *et al.* [41] who incorporated the use a periodic optical lattice (a periodic array of optical hotspots formed using optical holography) to deflect smaller particles preferentially and thus gradually sorting them towards one end of a microfluidic channel. Further intergration into the device architecture for biomedical applications by Wang *et al.* [17] demonstrated an optical force based cell sorting technique whereby radiation pressure was used to direct rare cells into a separate streams following detection via a fluorescent labeling method.

Although very complex manipulations have been demonstrated, the majority of optical tweezer based implementations rely on the ability to trap or not trap a particle based on whether the conditions for trapping stability are met [21-23]. Recently a number of works have extended these ideas to exploit the dependence of this trapping potential

on the particle properties, enabling much more advanced and subtle operations. In recent efforts, Imasaka and coworkers [25-28] provided the initial foundations for optically driven separation techniques, which they termed optical chromatography. In optical chromatography, [29] a loosely focused beam of light is incident on the particles of interest, resulting in the radiation pressure force that propulses them forward. The net impulse imparted to a larger particle is stronger than on a smaller particle, and therefore they will travel at different speeds and be separated. Recent demonstrations of optical separations include those by Hart *et al.* who have demonstrated refractive index separation of colloids [30] and other bioparticles [31]. This technique has also been integrated into microfluidic devices for pathogen detection [32], demonstrating very precise separation between very closely related bacteria species [33].

However, free space optofluidic transport systems are fundamentally limited in two significant ways. It is well known [34] that diffraction limits the degree to which light can be focused where the minimum focal width is given by:

$$d_{\min} = \frac{1.2\lambda}{\text{NA}} \quad (1.1)$$

where NA is the numerical aperture and λ is the wavelength. In an aqueous environment and a beam of light with a 850 nm wavelength and focused through a high numerical aperture the minimum spot size achievable is 550 nm. Since the radiation pressure force and gradient trapping force are a function of the spot intensity and optical intensity gradient, this represents a fundamental limitation on the propulsive forces that can be applied to a particle. In practice, the limitation affects the efficiency of both optical trapping and propulsion. The result is that free space optical traps can at smallest trap particles about 200 nm in diameter [30]. The limitation in

propulsion ability is due to a greatly reduced interaction length. Using Eq. 1.1 above, it is apparent that the most direct methods to decrease the area over which the optical energy is spread and increase the intensity are to either reduce the wavelength of the laser or increase the effective numerical aperture. In either case, the decrease in the spot size is necessarily offset by an equivalent decrease in the depth of focus. As such the interaction length, defined as the distance over which the optical impulse can be applied becomes small, making it impossible to perform optical transport over long distances. The reason why the traditional channel based transport techniques such as pressure driven flow or electrokinetics are useful is due to the fact that the impulse in those methods can be applied consistently over long distances.

1.3 Near-field and Evanescent Field Optical Manipulation

As stated previously, the short focal length and limited spot size are two major limitations of free space optical manipulations. One way to improve on the limitations imposed by the diffraction limit is through the use of near field methods [42], such as those based on the use of surface plasmonic resonances [43, 44] or other evanescent field techniques [45]. The advantage of these approaches is that the extremely high decay rate of the evanescent field leads to stronger trapping forces than can be achieved with free space systems. Examples include the work of Cizmar *et al.* [46] who demonstrated short range manipulation of 350 nm polystyrene beads and Grigorenko *et al.* [47] who used plasmonic resonance in surface bound metallic nanostructures to achieve high quality trapping of dielectric particles as small as 200nm in diameter. While in general these methods have in the past been successful at trapping and even assembling [48] small particles, similar to free space trapping, they are limited by the distance which they can transport objects, since the optical

manipulation region is limited by the field of view of the focused laser, and the plasmon propagation distance is relatively short.

Planar waveguides, and more specifically rectangular waveguides, are usually solid dielectric structures surrounded by materials and/or fluids with lower refractive index. Light can be guided within the solid core structures via total internal reflection. A ray of light confined in this fashion can propagate indefinitely within the waveguide structure. Unlike free-space systems, where the strong electric field gradients are only maintained near the beam waist, the mode profile in a waveguide structure is consistent along the entire length of the waveguide. In addition to the guided mode, there exists an evanescent mode which exponentially decays from the boundaries of the waveguide. The guiding mode contains the majority of the optical power and exists within the solid core of the waveguide. The evanescent mode, exists in the surrounding cladding regions, and decays spatially at an exponential rate as the distance from the core of the waveguide increases.

Trapping devices using waveguide structures as the source of the trapping force use solid core structures to sustain the guided mode, but employ a fluid cladding, such that particles suspended in solution can access the evanescent mode of the waveguide. The consistency of the modes allows for radiation pressure propulsion of particles along the length of a waveguide with a fluid cladding. However, since the evanescent mode contains only a fraction of the total power, only a small percentage (8 – 10%) is available for generating optical forces. This limitation is partially offset by a more confined gradient that does not require the use of high numerical aperture lenses and an indefinite interaction length. However, for applications requiring access to more of the optical mode, there is the possibility of using “liquid-core” waveguiding structures for optical transport. These types of systems often employ microfluidic flow

manipulation to meet the requirements for total internal reflection guiding in an all-liquid system, enabling access to the guided mode as well as the evanescent mode. Since the overlap between the guided mode and the transported optical energy is stronger in these systems, the potential exists for greater transport speeds. The most common configuration of such devices uses hydrodynamic focusing to flow fluids with different refractive indices next to each other while light is guided within the higher index core fluid [49]. Other examples include work by Mandal and Erickson [50] demonstrating the use of a specially tailored hollow core photonic crystal fiber (HCPCF) to propagate light within a liquid core environment and levitate dielectric particles. In a more chip-friendly format, Measor *et al.* [51] demonstrated the use of particle transport within a planar liquid core Anti-Resonant Reflective Optical Waveguides (ARROW) to characterize the optical performance of the waveguide.

The first experimental demonstrations of long distance optical transport on waveguides focused on the use of solid-core, fluid-clad structures which relied on the evanescent field of the waveguide to trap and transport suspended particles. These experiments showed the radiation pressure based propulsion on waveguides of particles of a variety of inorganic, metallic, and organic materials. Kawata and Sugiura [52], for example, first demonstrated the use of an evanescent field based optical trapping technique. This was further by Tanaka and Yamamoto [53], who showed the propulsion of polystyrene spheres on a channel waveguide.

While these seminal papers demonstrated for the first time the potential for using evanescent field trapping as a potential mechanism for optofluidic transport, it was unknown if the method would have the same versatility demonstrated for optical tweezers. Gaugiran *et al.* [54] demonstrated the use of silicon nitride waveguides for the propulsion of yeast and red blood cells. The proposed advantage in using silicon

nitride waveguides is the ability to guide light with a shorter wavelength of 1064 nm. More traditional optical waveguides constructed of silicon optimally guides light at 1550 nm wavelengths. The difference is that at 1064 nm the guided radiation is not heavily absorbed by water and can propagate with lower losses in a fluid-clad environment while also reducing the impact on biological species. The shorter wavelength also means that the guided mode is more strongly confined, leading to stronger trapping forces and higher propulsion velocities. Analogously, Ng *et al.* [55] demonstrated the propulsion of high absorption gold nanoparticles, using high absorption materials to generate larger propulsion velocities and trapping forces. In combination, these two papers provided experimental evidence of the diverse materials that could be transported on waveguiding structures. The first demonstration of an integrated microfluidic and waveguide transport experiment were conducted by Schmidt *et al.* [56] which showed the active trapping and propulsion of 3 μm polystyrene spheres on SU-8 polymer waveguides in PDMS microchannels. This paper also conducted the first experimental characterization of the steady-state propulsion velocities of trapped particles and examined the change in speed due to changes in particle size.

The advantage of using waveguide driven transport is that there are many types of devices that can be used to divert and alter the behavior of optical fields. Evanescent coupling can be used to cause light to effectively tunnel through a lower refractive index medium into an adjacent waveguide. Resonator devices allow for the attenuating properties of constructive and destructive interference to enable switching and/or creating highly focused hotspots in the guiding structure. There have been a few demonstrations of methods to manipulate the optical fields in waveguides for particle sorting/switching. Grujic *et al.* [37] first demonstrated using Y-branch waveguides as

a sorting mechanism for transported particles, shown in Figure 4. Polystyrene microparticles were guided down the “upper” or “lower” waveguides at the Y-split by altering the physical position of the input fiber, creating preferential pathways for particles to follow. An improvement over this type of device would be one that can divert the particles without physical movement such as by changing the wavelength of the input light, and thus increase the switching time. The ideal goal here would be to develop a passive mechanism which would divert particles based on their intrinsic properties rather than an active switching method.

1.4 Theory of Optofluidic Transport

This section covers a theoretical description of optofluidic transport and relevant fundamental phenomena that will be discussed in this dissertation. After a brief review of significant contributions to the theoretical literature, I will present an overview of the relevant microscale fluid mechanics and the behavior of small particles suspended in a fluid environment. The second section describes the general electromagnetic and guided wave optics theory required to describe optical forces, focusing on the Rayleigh scattering solution and a more comprehensive solution using the Maxwell’s Stress Tensor.

Optofluidic transport is in its most fundamental form a combination of hydrodynamics and electromagnetic theory. Because of the strong application focus of the research conducted in this area, much of the theory is tailored to understanding the specific geometries and cases that arise in experimental research. In the case of electromagnetics, the Rayleigh and Mie scattering theories are often used to explain the propulsion and trapping forces exerted on particles in optofluidic systems within an optical field. The Mie and Rayleigh theories are specific towards evaluating the forces exerted on particles in the presence of an optical field. As might be expected,

the major approximations of these theories assume a spherical scatterer and relatively non-complex geometries. The main difference is that Rayleigh scattering theory [57] is designed to treat particles which are much smaller than the wavelength of light incident upon it, while Mie theory [58] treats larger particles which exhibits different scattering behavior from Rayleigh particles. Almaas and Brevik [59] and Ng *et al.* [60] also both deal specifically with the behavior of particles in evanescent fields. Fluid dynamics of optofluidic systems generally consider the case of strongly laminar flow allowing a number of simplifications to the problem. The influence of fluid forces on particle transport can be reduced to an analytical Stokes drag law or Faxen's Law expression. A concise summary of both optical and hydrodynamic forces within the context of optical tweezing is provided by Svoboda and Block [61]. Readers interested in the behavior of metallic particles in optical fields are directed to another paper by Svoboda [30] and another by Gaugiran *et al.* [62].

With the development of multiphysics based simulation software packages, recent thrusts in understanding the behavior of particles have focused on using more general derivations of optical forces, such as the Maxwell Stress Tensor [63], and using simulation to evaluate optical and hydrodynamic forces in non-trivial geometries. In particular, Gaugiran *et al.* [54] first used finite element simulation to estimate the propulsion and trapping forces on rectangular waveguides. This was expanded further upon by Yang and Erickson [64], combining the finite element method and a comprehensive analysis of the optical forces using the Maxwell Stress Tensor to detail a theory of optofluidic trapping stability in systems with fluid drag and optical trapping forces. In a recent publication demonstrating self-induced back-action (SIBA) trapping, Juan *et al.* [65] showed that when the particle forms an active component of

the trap, a comprehensive method using the Maxwell Stress Tensor is more accurate than using a Rayleigh expression.

Conservation of mass and momentum are the fundamental laws that drive the behavior of all fluids. Mathematically these laws are represented by the conservation of mass and Navier-Stokes equations [66]. To reduce the complexity of the equations and to make analytical solutions for microfluidics possible, a few key assumptions are made about the fluid and system. The fluid is assumed to be Newtonian, such that the fluid is incompressible and of constant viscosity, which is generally true for most liquids of interest in microfluidics. Transport is also assumed to occur under conditions of low Reynolds number, $Re = \rho Ua/\mu$, where ρ is the fluid density, U is the characteristic transport speed, a is an appropriate size scale and μ is the viscosity. For pure particle transport in a quiescent medium, U would be the particle speed and a would be its diameter. A low Reynolds number generally means that momentum transport occurs through diffusion rather than convection and that the non-linear terms inertial terms in the Navier Stokes equations can be ignored. Under these assumptions the more general conservation of mass and Navier-Stokes equations reduce to conservation of volume (Eq. 1.2) and the Stokes equation (Eq. 1.3):

$$\nabla \cdot \mathbf{v} = 0 \tag{1.2}$$

$$\mu \nabla^2 \mathbf{v} - \nabla P = 0 \tag{1.3}$$

where \mathbf{v} is the velocity field and P is the pressure.

1.4.1 Hydrodynamic forces on a particle in a flow

Generally speaking a particle in a flow will experience a net pressure force caused by pressure drop across the particle and a friction force caused by the flow of a viscous liquid over the surface. In the most general case, the net drag force can be written as

$$\mathbf{F}_D = \oint_S \mathbf{T}_F \cdot \mathbf{n} \, dS \quad (1.4)$$

where \mathbf{F}_D is the drag force, \mathbf{T}_F is the fluid stress tensor, and \mathbf{n} is the normal vector to the surface of the particle. For an incompressible Newtonian fluid, the stress tensor is written as:

$$\mathbf{T}_F = -P\mathbf{I} + \mu(\nabla\mathbf{v} + \nabla\mathbf{v}^T) \quad (1.5)$$

where \mathbf{I} is the isotropic tensor and $\nabla\mathbf{v}$ is the gradient of the flow velocity.

The above form of the hydrodynamic equations is appropriate for use in numerical simulations, but difficult to manipulate analytically. For two relevant cases involving drag on a sphere, an analytical solution is available. The simpler of the two describes the drag experienced by a spherical object moving through a stagnant fluid in an infinite domain. In such a case Eq. 1.4 reduces to the expression shown below, known commonly as Stokes drag:

$$\mathbf{F}_D = -6\pi\mu aU \quad (1.6)$$

where U is the velocity of the particle relative to the bulk flow and a is the particle radius. This equation is only accurate when a particle is far from any no-slip boundaries. For a case more relevant to optofluidic transport on a waveguide, it can be shown that a modification of the Stokes drag equation can be made to approximate

the drag for a particle moving near an infinite solid surface. This equation, known as Faxen's Law [61, 67] is given as:

$$\mathbf{F}_D = \frac{-6\pi\mu a U}{\left[1 - \frac{9}{16}\left(\frac{a}{h}\right) + \frac{1}{8}\left(\frac{a}{h}\right)^3 - \frac{45}{256}\left(\frac{a}{h}\right)^4 - \frac{1}{16}\left(\frac{a}{h}\right)^5\right]} \quad (1.7)$$

where h is the distance between the particle center and the wall surface. Eq. 1.7 is generally true for any particle near an infinite surface, but in the case of waveguides where there is a finite width, Faxen's Law strictly applies only in the cases where the particle diameter is much smaller than the width of the waveguide, $2a \ll w$, where w is the width of the waveguide.

1.4.2 Solution of wave equation for dielectric slab waveguide

The most general equations that govern the behavior of light in any situation are the Maxwell's Equations. In the case for a system with no current flux or static charges, the Maxwell's equations are given as:

$$\begin{aligned} \nabla \times \mathbf{E} &= -\frac{\partial \mathbf{B}}{\partial t} \\ \nabla \times \mathbf{H} &= \frac{\partial \mathbf{D}}{\partial t} \\ \nabla \cdot \mathbf{B} &= 0 \\ \nabla \cdot \mathbf{D} &= 0 \end{aligned} \quad (1.8)$$

where \mathbf{E} is the electric field, \mathbf{B} is the magnetic flux, \mathbf{D} is the electric flux, and \mathbf{H} is the magnetic field. It can be shown that for a constant electric permittivity (ϵ) and magnetic permeability (μ), the four Maxwell's equations can be simplified into a single partial differential equation, the electromagnetic wave equation:

$$\nabla^2 \mathbf{E} - \mu \varepsilon \frac{\partial^2 \mathbf{E}}{\partial t^2} = 0 \quad (1.9)$$

This sub-section covers the solution of the wave equation for a planar dielectric slab waveguide, which consists of a slab of higher refractive index material ($n^2 = \varepsilon$) sandwiched by two slabs of lower index material. In the simplest case, the system is symmetric, and the two cladding regions have the same refractive index. Depending on the width of the waveguide and the refractive index contrast ($n_{\text{waveguide}} - n_{\text{cladding}}$) of the system, there can be multiple solutions to the wave equation with regard to the transverse spatial distribution of the electric field. Each of these solutions corresponds to a mode of the waveguide. The focus here will be on waveguides that can only sustain the most fundamental mode of propagation, called single-mode waveguides.

It is well known that light propagates as a sinusoidal wave in space. Therefore, if the solution of the wave equation is assumed to take the form of:

$$E(y, z) = E_A A_E(y) \exp(-i\beta z) \quad (1.10)$$

Where E_A is an arbitrary constant, A_E is the complex amplitude of the wave or the transverse amplitude variation of the electric field, z is position along the propagation axis, y is the position along the transverse axis, and β is the propagation constant of the wave. In the case of a dielectric slab waveguide there is a step change in the refractive index at the boundary between the waveguide and the cladding. To maintain continuity of the electric flux field, a different solution is found for the field within and external to the waveguide. The internal field distribution for a single-mode waveguide is:

$$A_{E_{\text{int}}} y = \cos\left(\frac{2\pi \sin \theta_m}{\lambda} y\right) \quad (1.11)$$

Where θ_m is the angle of reflection of the mode and λ is the wavelength. This solution is only valid for the fundamental mode ($m = 0$) and all even modes. The solution for odd modes replaces cosine for sine. It can also be shown that the external field, which resides in the cladding layers, takes the form of an exponentially decaying wave:

$$A_{E_{\text{ext}}}(y) = \begin{cases} \exp -\gamma_m y , & y > \frac{d}{2} \\ \exp \gamma_m y , & y < -\frac{d}{2} \end{cases} \quad (1.12)$$

Where d is the width of the waveguide and γ_m is the extinction coefficient of the evanescent mode, and governs the spatial decay of the field as a function of distance away from the waveguide. This wave is what was previously referred to as the evanescent mode of the waveguide.

1.4.3 Electromagnetic forces on a particle

The total optical force exerted on a particle in an electromagnetic field can be decomposed into two main components. The optical trapping force acts to pull a particle along the gradient of the electric field towards the region of highest optical intensity. This effect is due to a temporary polarization of the particle which creates a Lorenz force resulting in a pulling force along the gradient of the field. The radiation pressure forces are due to the scattering and absorption of photons on the particle which pushes particles in the direction of optical intensity. As described by Mishchenko *et al.* [68], this is an orthogonal decomposition of the total force that is more generally described by the surface integral of the time averaged Maxwell stress tensor, $\langle \mathbf{T}_M \rangle$ as shown in Eq. 1.13:

$$\langle \mathbf{T}_M \rangle = \mathbf{D}\mathbf{E}^* + \mathbf{H}\mathbf{B}^* - \frac{1}{2} \mathbf{D} \cdot \mathbf{E}^* + \mathbf{H} \cdot \mathbf{B}^* \mathbf{I} \quad (1.13)$$

where \mathbf{E} is the electric field, \mathbf{B} is the magnetic flux field, \mathbf{D} is the electric displacement, \mathbf{H} is the magnetic field, \mathbf{E}^* and \mathbf{B}^* are the complex conjugates and \mathbf{I} is the isotropic tensor. The time averaged Maxwell stress tensor is appropriate here since any transport processes occur on time scales much longer than the optical period [69]. When expanded out, Eq. 1.13 becomes:

$$\langle \mathbf{T}_M \rangle = \begin{pmatrix} D_x E_x^* + B_x H_x^* - \frac{1}{2} \mathbf{D} \cdot \mathbf{E}^* + \mathbf{B} \cdot \mathbf{H}^* & D_x E_y^* + B_x H_y^* & D_x E_z^* + B_x H_z^* \\ D_y E_x^* + B_y H_x^* & D_y E_y^* + B_y H_y^* - \frac{1}{2} \mathbf{D} \cdot \mathbf{E}^* + \mathbf{B} \cdot \mathbf{H}^* & D_y E_z^* + B_y H_z^* \\ D_z E_x^* + B_z H_x^* & D_z E_y^* + B_z H_y^* & D_z E_z^* + B_z H_z^* - \frac{1}{2} \mathbf{D} \cdot \mathbf{E}^* + \mathbf{B} \cdot \mathbf{H}^* \end{pmatrix} \quad (1.14)$$

where the subscripts x, y and z are the coordinate directions. By integrating the time-independent Maxwell stress tensor on a surface enclosing a particle, we can determine the total electromagnetic force acting on the system, \mathbf{F}_{EM} , given by:

$$\mathbf{F}_{EM} = \oint_s \langle \mathbf{T}_M \rangle \cdot \mathbf{n} \, dS \quad (1.15)$$

where \mathbf{n} is the unit vector normal to the particle surface. As we, [70] and others [54], have shown the \mathbf{E} and \mathbf{H} fields can be computed either through a full solution to Maxwell's equations or by solving the time harmonic wave equation via the Finite Element Method and the integration of Eq. 1.15 carried out numerically.

The above set of equations represent a relatively basic, but general, model for optofluidic transport, ignoring such effects as heating, surface friction, electrical double layer repulsion. Despite this the basic model has proven to be relatively predictive of observed experimental behaviors [56]. The model can be simplified for

two special cases of optofluidic transport: (1) when the transported particle radius, a , is much smaller than the wavelength of light, λ , which is applicable in nanophotonic devices and (2) when the particle radius is approximately the same or much larger than λ .

1.4.4 Optofluidic transport for Rayleigh particles

This first regime discussed uses the case where the transported particle can be considered to meet to conditions for Rayleigh light scattering. The particle of interest must be much smaller than the wavelength of light, and furthermore the electromagnetic field surrounding the particle must be uniform. For wavelengths in the range of 1000 – 1550 nm, this is generally true for particles smaller than 100 nm in diameter. For this case the scattering, adsorption and trapping forces exerted on a particle [30][[60, 71, 72] take an analytical form, given as:

$$F_{scat} = \frac{8\pi^3 I_o \alpha^2 \epsilon_m^{5/2}}{3c\lambda^4} \quad (1.16)$$

$$F_{abs} = \frac{2\pi\epsilon_m I_o}{c\lambda} \text{Im}(\alpha) \quad (1.17)$$

$$F_{trap} = \frac{n_m \alpha}{2c} \nabla I_o \quad (1.18)$$

where $\alpha = 3V(\epsilon - \epsilon_m)/(\epsilon + 2\epsilon_m)$ is the polarizability of the particle, V is the particle volume, c is the speed of light, ϵ_p and ϵ_m are the dielectric constants of the particle and material and I_o is the optical intensity. Equating F_{scat} and F_{abs} with Stokes drag from Eq. 1.6 we obtain:

$$U_o = \frac{n_m k_m I_o}{6\pi a c \eta} \left(\frac{k_m^3 \alpha^2}{6\pi} + \text{Im}(\alpha) \right) \quad (1.19)$$

where $k_m = 2\pi n_m/\lambda$ and is descriptive of the steady state transport velocity for particles in the Rayleigh regime. In the specific case of a particle near the surface of a waveguide, Eq. 1.19 can be improved by countering the propulsion forces with the Faxen's law drag force, Eq. 1.7, however it is generally difficult to estimate the distance the particle is above the waveguide. A conservative estimate however could be obtained by assuming the particle was right near the surface, in which case $a=h$.

1.4.5 Optofluidic transport for non-Rayleigh particles

For many cases of optical tweezing or particle trapping on waveguides, the particle size is much larger than the optical wavelength or the field acting on the particle is sufficiently non-uniform and therefore one of the two assumptions for using the Rayleigh equations described previously are broken. While there are some theories, such as Mie theory, that can describe how light scatters and how momentum transfers to the particle, these are generally only applicable to the most general and basic scenarios. Analysis of more specific cases such as evanescent field trapping requires a numerical method to simulate the optical field and calculate the trapping forces and propulsion velocity. Specifically, the electromagnetic fields can be computed either through a full solution of Maxwell's equations or by solving the time harmonic wave equation via a Finite Element Method. Once these solutions are obtained, Eq. 1.15 (the Maxwell Stress Tensor) can be solved to obtain the net electromagnetic force on the particle, in all three coordinate directions, as a function of the optical power in the waveguide. Tracking particle motion in a fluid is a relatively complex simulation and requires large amounts of computing power. As an alternative, the net drag on a particle is calculated by shifting reference frames and keeping the particle still while applying boundary conditions that simulate the flow moving by it. In the low Reynolds number regime the drag force is linearly proportion to the flow velocity so to determine the

particle drag a “slip” velocity boundary condition is applied on all surfaces opposite the direction one expects the particle to move. The drag force is obtained by integrating Eq. 1.4 over the particle surface and the total force can be scaled to the particle speed by dividing by the imposed slip velocity. For scenarios where the flow is incident on the particle, the boundary conditions should match those needed to simulate the type of flow (pressure driven flow, electrokinetic).

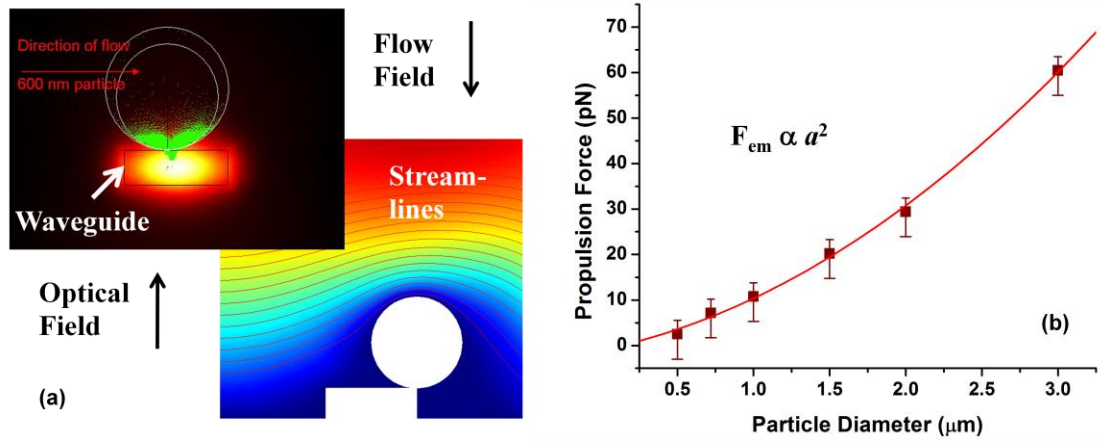


Figure 1.1: Forces on a particle trapped on a waveguide. (a) Cross section of guided mode in the waveguide and streamlines for a particle trapped on the waveguide and subject to a cross flow. (b) Propulsion force computed on particles trapped on the waveguide.

Figure 1.1 shows the results of finite element based computations to calculate the trapping and fluid drag forces for a microsphere trapped on a waveguide structure. In this case, the diameter is much larger than the wavelength and the electric field is non-uniform. From Figure 1.1(b) it is apparent that the propulsive force follows an approximate squared relation with particle size and that \mathbf{F}_{EM} (the electromagnetic force) is also proportional to the optical intensity. As such it is reasonable to qualitatively approximate $\mathbf{F}_{EM,scat} = C_1 a^2 I_o$, where C_1 is a constant and an unknown function of the physical parameters of the system and I_o is the optical intensity. Using the Faxen’s Law approximation $\mathbf{F}_{flow} = 6\pi\eta a U \mathcal{O}(a/h)$, where $g(a/h)$ is the

denominator in Eq. 1.7. If the distance between the bottom of the particle and the top of the waveguide is small compared to the particle diameter, such that $a/h \sim 1$ then $g(a/h)$ is constant and we can derive the following approximate equation descriptive of the transport velocity,

$$U_o = \frac{C_1 a^2 I}{6\pi\eta a/g(a/h)} = C_2 \frac{aI_o}{\eta} \quad (1.20)$$

where C_2 is a different constant comprising of the same system physical parameters as C_1 . Compared to Eq. 1.19, the transport velocity in the non-Rayleigh regime appears to contain only a linear dependence on particle size compared to the much stronger dependence exhibited by particles that are within the Rayleigh regime.

REFERENCES

- [1] D. M. Audet and W. L. Olbricht, "The Motion of Model Cells at Capillary Bifurcations," *Microvascular Research*, **33**, 377-396, (1987).
- [2] U. Y. Schaff, M. M. Q. Xing, K. K. Lin, N. Pan, N. L. Jeon, and S. I. Simon, "Vascular mimetics based on microfluidics for imaging the leukocyte-endothelial inflammatory response," *Lab on a Chip*, **7**, 448-456, (2007).
- [3] C. D. Chin, V. Linder, and S. K. Sia, "lab-on-a-chip devices for global health: Past studies and future opportunities," *Lab on a Chip*, **7**, 41-57, (2007).
- [4] A. Manz, N. Graber, and H. M. Widmer, "Miniaturized Total Chemical-Analysis Systems - a Novel Concept for Chemical Sensing," *Sensors and Actuators B-Chemical*, **1**, 244-248, (1990).
- [5] J. A. Jensen, J. Mathorne, T. Gravesen, and B. Stage, "Deconvolution of in-Vivo Ultrasound B-Mode Images," *Ultrasonic Imaging*, **15**, 122-133, (1993).
- [6] E. Verpoorte, "Microfluidic chips for clinical and forensic analysis," *Electrophoresis*, **23**, 677-712, (2002).
- [7] T. Vo-Dinh and B. Cullum, "Biosensors and biochips: advances in biological and medical diagnostics," *Fresenius Journal of Analytical Chemistry*, **366**, 540-551, (2000).
- [8] S. C. Terry, J. H. Jerman, and J. B. Angell, "Gas-Chromatographic Air Analyzer Fabricated on a Silicon-Wafer," *Ieee Transactions on Electron Devices*, **26**, 1880-1886, (1979).
- [9] A. D. Stroock, S. K. W. Dertinger, A. Ajdari, I. Mezic, H. A. Stone, and G. M. Whitesides, "Chaotic mixer for microchannels," *Science*, **295**, 647-651, (2002).
- [10] J. S. Marcus, W. F. Anderson, and S. R. Quake, "Microfluidic single-cell mRNA isolation and analysis," *Analytical Chemistry*, **78**, 3084-3089, (2006).
- [11] Y. A. Song, S. Hsu, A. L. Stevens, and J. Y. Han, "Continuous-flow pl-based sorting of proteins and peptides in a microfluidic chip using diffusion potential," *Analytical Chemistry*, **78**, 3528-3536, (2006).
- [12] A. R. Wheeler, H. Moon, C. J. Kim, J. A. Loo, and R. L. Garrell, "Electrowetting-based microfluidics for analysis of peptides and proteins by matrix-assisted laser desorption/ionization mass spectrometry," *Analytical Chemistry*, **76**, 4833-4838, (2004).
- [13] A. J. Tudos, G. A. J. Besselink, and R. B. M. Schasfoort, "Trends in miniaturized total analysis systems for point-of-care testing in clinical chemistry," *Lab on a Chip*, **1**, 83-95, (2001).

- [14] T. Chovan and A. Guttman, "Microfabricated devices in biotechnology and biochemical processing," *Trends in Biotechnology*, **20**, 116-122, (2002).
- [15] M. A. Unger, H. P. Chou, T. Thorsen, A. Scherer, and S. R. Quake, "Monolithic microfabricated valves and pumps by multilayer soft lithography," *Science*, **288**, 113-116, (2000).
- [16] R. J. Hunter, *Zeta potential in colloid science: principles and applications*. London: Academic Press, 1981.
- [17] J. Lyklema, *Fundamentals of Interface and Colloid Science, Volume 1: Fundamentals* vol. 1. London: Academic Press, 1991.
- [18] J. Lyklema, *Fundamentals of Interface and Colloid Science, Volume 2: Solid Liquid Interfaces*. London: Academic Press, 1995.
- [19] D. Li, *Electrokinetics in Microfluidics* Boston: Elsevier Academic 2004.
- [20] N. Krishnan, N. Agrawal, M. A. Burns, and V. M. Ugaz, "Reactions and fluidics in miniaturized natural convection systems," *Analytical Chemistry*, **76**, 6254-6265, (2004).
- [21] Y. Xiang and H. H. Bau, "Complex magnetohydrodynamic low-Reynolds-number flows," *Physical Review E*, **68**, 2003).
- [22] J. Zeng and T. Kormeyer, "Principles of droplet electrohydrodynamics for lab-on-a-chip," *Lab on a Chip*, **4**, 265-277, (2004).
- [23] A. A. Darhuber, J. P. Valentino, S. M. Troian, and S. Wagner, "Thermocapillary actuation of droplets on chemically patterned surfaces by programmable microheater arrays," *Journal of Microelectromechanical Systems*, **12**, 873-879, (2003).
- [24] H. A. Stone, A. D. Stroock, and A. Ajdari, "Engineering flows in small devices: Microfluidics toward a lab-on-a-chip," *Annual Review of Fluid Mechanics*, **36**, 381-411, (2004).
- [25] N. Nguyen and S. Wereley, *Fundamentals and Applications of Microfluidics*. New York: Artech House, 2002.
- [26] S. Ghosal, "Electrokinetic flow and dispersion in capillary electrophoresis," *Annual Review of Fluid Mechanics*, **38**, 309-338, (2006).
- [27] D. Erickson, D. Sinton, and D. Q. Li, "Joule heating and heat transfer in poly(dimethylsiloxane) microfluidic systems," *Lab on a Chip*, **3**, 141-149, (2003).
- [28] A. Ashkin, "Acceleration and Trapping of Particles by Radiation Pressure," *Physical Review Letters*, **24**, 156-&, (1970).

- [29] A. Ashkin and J. M. Dziedzic, "Optical Trapping and Manipulation of Viruses and Bacteria," *Science*, **235**, 1517-1520, (1987).
- [30] K. Svoboda and S. M. Block, "Optical Trapping of Metallic Rayleigh Particles," *Optics Letters*, **19**, 930-932, (1994).
- [31] S. Chu and C. Wieman, "Laser Cooling and Trapping of Atoms," *Journal of the Optical Society of America B-Optical Physics*, **6**, 2020-2020, (1989).
- [32] P. K. Wong, Y. K. Lee, and C. M. Ho, "Deformation of DNA molecules by hydrodynamic focusing," *Journal of Fluid Mechanics*, **497**, 55-65, (2003).
- [33] C. Monat, P. Domachuk, and B. J. Eggleton, "Integrated optofluidics: A new river of light," *Nature Photonics*, **1**, 106-114, (2007).
- [34] D. Psaltis, S. R. Quake, and C. H. Yang, "Developing optofluidic technology through the fusion of microfluidics and optics," *Nature*, **442**, 381-386, (2006).
- [35] L. N. Jiang and S. Pau, "Integrated waveguide with a microfluidic channel in spiral geometry for spectroscopic applications," *Applied Physics Letters*, **90**, 111108, (2007).
- [36] D. Erickson, T. Rockwood, T. Emery, A. Scherer, and D. Psaltis, "Nanofluidic tuning of photonic crystal circuits," *Optics Letters*, **31**, 59-61, (2006).
- [37] K. Grujic, O. G. Helleso, J. P. Hole, and J. S. Wilkinson, "Sorting of polystyrene microspheres using a Y-branched optical waveguide," *Optics Express*, **13**, 1-7, (2005).
- [38] M. M. Wang, E. Tu, D. E. Raymond, J. M. Yang, H. C. Zhang, N. Hagen, B. Dees, E. M. Mercer, A. H. Forster, I. Kariv, P. J. Marchand, and W. F. Butler, "Microfluidic sorting of mammalian cells by optical force switching," *Nature Biotechnology*, **23**, 83-87, (2005).
- [39] S. J. Hart, A. Terray, J. Arnold, and T. A. Leski, "Sample concentration using optical chromatography," *Optics Express*, **15**, 2724-2731, (2007).
- [40] R. W. Applegate, J. Squier, T. Vestad, J. Oakey, D. W. M. Marr, P. Bado, M. A. Dugan, and A. A. Said, "Microfluidic sorting system based on optical waveguide integration and diode laser bar trapping," *Lab on a Chip*, **6**, 422-426, (2006).
- [41] M. P. MacDonald, G. C. Spalding, and K. Dholakia, "Microfluidic sorting in an optical lattice," *Nature*, **426**, 421-424, (2003).
- [42] K. Dholakia and P. J. Reece, "Near-Field Optical Micromanipulation," in *Structured Light and Its Applications*, D. L. Andrews, Ed. Amsterdam: Academic Press, 2008, pp. 107-138.

- [43] M. Righini, A. S. Zelenina, C. Girard, and R. Quidant, "Parallel and selective trapping in a patterned plasmonic landscape," *Nature Physics*, **3**, 477-480, (2007).
- [44] R. F. Marchington, M. Mazilu, S. Kuriakose, V. Garces-Chavez, P. J. Reece, T. F. Krauss, M. Gu, and K. Dholakia, "Optical deflection and sorting of microparticles in a near-field optical geometry," *Optics Express*, **16**, 3712-3726, (2008).
- [45] M. Gu, J. B. Haumonte, Y. Micheau, J. W. M. Chon, and X. S. Gan, "Laser trapping and manipulation under focused evanescent wave illumination," *Applied Physics Letters*, **84**, 4236-4238, (2004).
- [46] T. Cizmar, M. Siler, M. Sery, P. Zemanek, V. Garces-Chavez, and K. Dholakia, "Optical sorting and detection of submicrometer objects in a motional standing wave," *Physical Review B*, **74**, 2006).
- [47] A. N. Grigorenko, N. W. Roberts, M. R. Dickinson, and Zhang Y, "Nanometric optical tweezers based on nanostructured substrates," *Nat Photon*, **2**, 365-370, (2008).
- [48] V. Garces-Chavez, R. Quidant, P. J. Reece, G. Badenes, L. Torner, and K. Dholakia, "Extended organization of colloidal microparticles by surface plasmon polariton excitation," *Physical Review B*, **73**, 2006).
- [49] S. K. Y. Tang, B. T. Mayers, D. V. Vezenov, and G. M. Whitesides, "Optical waveguiding using thermal gradients across homogeneous liquids in microfluidic channels," *Applied Physics Letters*, **88**, -, (2006).
- [50] S. Mandal and D. Erickson, "Optofluidic Transport in Liquid Core Waveguiding Structures," *Applied Physics Letters*, **90**, 184103, (2007).
- [51] P. Measor, S. Kuehn, E. J. Lunt, B. S. Phillips, A. R. Hawkins, and H. Schmidt, "Hollow-core waveguide characterization by optically induced particle transport," *Optics Letters*, **33**, 672-674, (2008).
- [52] S. Kawata and T. Sugiura, "Movement of Micrometer-Sized Particles in the Evanescent Field of a Laser-Beam," *Optics Letters*, **17**, 772-774, (1992).
- [53] T. Tanaka and S. Yamamoto, "Optically induced propulsion of small particles in an evenescent field of higher propagation mode in a multimode, channeled waveguide," *Applied Physics Letters*, **77**, 3131-3133, (2000).
- [54] S. Gaugiran, S. Getin, J. M. Fedeli, G. Colas, A. Fuchs, F. Chatelain, and J. Derouard, "Optical manipulation of microparticles and cells on silicon nitride waveguides," *Optics Express*, **13**, 6956-6963, (2005).

- [55] L. N. Ng, B. J. Luff, M. N. Zervas, and J. S. Wilkinson, "Propulsion of gold nanoparticles on optical waveguides," *Optics Communications*, **208**, 117-124, (2002).
- [56] B. S. Schmidt, A. H. Yang, D. Erickson, and M. Lipson, "Optofluidic trapping and transport on solid core waveguides within a microfluidic device," *Opt. Express*, **15**, 14322-14334, (2007).
- [57] Y. Harada and T. Asakura, "Radiation forces on a dielectric sphere in the Rayleigh scattering regime," *Optics Communications*, **124**, 529-541, (1996).
- [58] H. Y. Jaising and O. G. Helleso, "Radiation forces on a Mie particle in the evanescent field of an optical waveguide," *Optics Communications*, **246**, 373-383, (2005).
- [59] E. Almaas and I. Brevik, "Radiation forces on a micrometer-sized sphere in an evanescent field," *Journal of the Optical Society of America B-Optical Physics*, **12**, 2429-2438, (1995).
- [60] L. N. Ng, B. J. Luf, M. N. Zervas, and J. S. Wilkinson, "Forces on a Rayleigh particle in the cover region of a planar waveguide," *Journal of Lightwave Technology*, **18**, 388-400, (2000).
- [61] K. Svoboda and S. M. Block, "Biological Applications of Optical Forces," *Annual Review of Biophysics and Biomolecular Structure*, **23**, 247-285, (1994).
- [62] S. Gaugiran, S. Getin, J. M. Fedeli, and J. Derouard, "Polarization and particle size dependence of radiative forces on small metallic particles in evanescent optical fields. Evidences for either repulsive or attractive gradient forces," *Optics Express*, **15**, 8146-8156, (2007).
- [63] J. D. Jackson, *Classical electrodynamics*, 2d ed. New York: Wiley, 1975.
- [64] A. H. J. Yang and D. Erickson, "Stability analysis of optofluidic transport on solid-core waveguiding structures," *Nanotechnology*, **19**, 045704, (2008).
- [65] M. L. Juan, R. Gordon, Y. J. Pang, F. Eftekhari, and R. Quidant, "Self-induced back-action optical trapping of dielectric nanoparticles," *Nature Physics*, **5**, 915-919, (2009).
- [66] R. L. Panton, *Incompressible flow*, 3rd ed. Hoboken, N.J.: J. Wiley, 2005.
- [67] J. Happel and H. Brenner, *Low Reynolds number hydrodynamics, with special applications to particulate media*, 2d rev. ed. Leyden,: Noordhoff International Publishing, 1973.
- [68] M. Mishchenko, L. Travis, and A. Lacis, *Scattering, absorption, and emission of light by small particles*. Cambridge: Cambridge University Press, 2002.

- [69] I. Brevik, T. A. Sivertsen, and E. Almaas, "Radiation forces on an absorbing micrometer-sized sphere in an evanescent field," *Journal of the Optical Society of America B-Optical Physics*, **20**, 1739-1749, (2003).
- [70] A. J. H. Yang and D. Erickson, "Stability analysis of optofluidic transport on solid-core waveguiding structures.," *Nanotechnology*, **19**, 045704, (2008).
- [71] L. N. Ng, M. N. Zervas, J. S. Wilkinson, and B. J. Luff, "Manipulation of colloidal gold nanoparticles in the evanescent field of a channel waveguide," *Applied Physics Letters*, **76**, 1993-1995, (2000).
- [72] K. C. Neuman and S. M. Block, "Optical trapping," *Review of Scientific Instruments*, **75**, 2787-2809, (2004).

2.0 Optical Manipulation of Nanoparticles and Biomolecules in Sub-Wavelength Slot Waveguides*

The ability to manipulate nanoscopic [1-4] matter precisely is critical for the development of active nanosystems. Optical tweezers are excellent tools for transporting particles ranging in size from several micrometres to a few hundred nanometres. Manipulation of dielectric objects with much smaller diameters, however, requires stronger optical confinement and higher intensities than can be provided by these diffraction-limited [5] systems. Here we present an approach to optofluidic transport that overcomes these limitations, using subwavelength liquid-core slot waveguides [6]. The technique simultaneously makes use of near-field optical forces to confine matter inside the waveguide and scattering/adsorption forces to transport it. The ability of the slot waveguide to condense the accessible electromagnetic energy to scales as small as 60 nm allows us also to overcome the fundamental diffraction problem. We apply the approach here to the trapping and transport of 75-nm dielectric nanoparticles and 1-DNA molecules. Because trapping occurs along a line, rather than at a point as with traditional point traps [7, 8], the method provides the ability to handle extended biomolecules directly. We also carry out a detailed numerical analysis that relates the near-field optical forces to release kinetics. We believe that the architecture demonstrated here will help to bridge the gap between optical manipulation and nanofluidics.

* This chapter was previously published in A. H. J. Yang, S. D. Moore, B. S. Schmidt, M. Klug, M. Lipson, and D. Erickson, "Optical manipulation of nanoparticles and biomolecules in sub-wavelength slot waveguides," *Nature*, **457**, 71-75, (2009). Reproduced with permission from the Nature Publishing Group.

In a series of recent articles, Psaltis *et al.* [9] and Monat *et al.* [10] describe the enormous potential of integrating optical and microfluidic elements into ‘lab-on-a-chip’ devices, particularly in improving fluid and particle manipulations. Traditionally accomplished through direct particle manipulation with laser tweezers[1-3, 11] or indirectly using optically induced microfluidic effects [12, 13], the precision with which particles can be manipulated with these techniques makes them particularly useful for applications ranging from flow cytometry [3, 14] to self-assembly [15]. Fundamentally, however, these free-space systems are limited in two ways. First, diffraction limit show tightly the light can be focused and thereby limits the overall strength of the trap. Second, the trapping region has a very short focal depth, preventing the continuous transport of nanoparticles by means of radiation pressure.

To improve trapping stability, a number of near-field methods have recently been developed [16-18]. Examples are the use of interfering Gaussian beams reflected off a prism surface to sort 350-nm polystyrene beads [19], and the use of localized plasmonic resonances in surface-bound metallic nanostructures to trap 200-nm dielectric particles [4]. Waveguide-based optical transport [20, 21] is analogous to these near-field methods in that the evanescent field extending into the surrounding liquid serves to attract particles to the waveguide. However, particles also experience photon scattering and absorption forces which propel them along it for a distance limited only by the losses in the system. Recent efforts in this area have demonstrated the sustained propulsion of dielectric microparticles [21, 22], metallic nanoparticles [23, 24], and cells [25]. The limitation that prevents these systems from manipulating smaller matter, including biomolecules, is that the particles only interact with the small portion of total transported light because most of it is confined within the solid core of the waveguide.

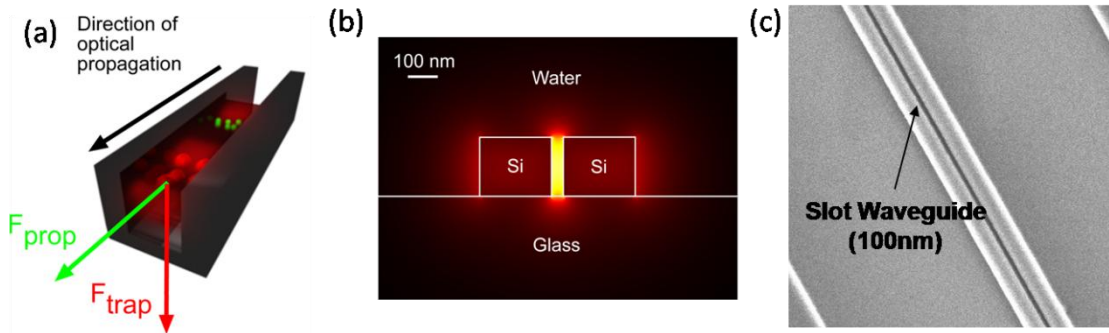


Figure 2.1: Nanoscale optofluidic transport. (a) Schematic illustrating the transport of two different sizes of nanoparticles in a slot waveguide. The force F_{prop} represents the radiation pressure force responsible for optofluidic transport, and F_{trap} is the trapping force that holds nanoparticles within the slot region. (b) Mode profile for a silicon-on-insulator 40-nm slot waveguide immersed in water, calculated using a finite-element simulation package. The main trapping region is in the high-intensity slot mode, although alternate trapping locations are located on the sides of the waveguide, where there are two decaying evanescent modes. (c) Scanning electron microscope image of 100-nm slot waveguide structure

Recently Almeida *et al.* [6] developed a nanophotonic structure, known as a slot waveguide, that can overcome this challenge. Illustrated in Figure 1, the slot waveguide comprises a nanoscale slot sandwiched between two materials of much higher refractive index. As shown in Figure 1b, there exists a pseudo-transverse-electric (TE) mode that has a large electric field discontinuity at the horizontal boundaries of the slot region. The result is a high-intensity eigenmode in the slot making the majority of the optical energy accessible within the low-index fluid region. Here we demonstrate the use of these subwavelength-scale slot waveguides for optical capture, trapping and transport of both dielectric nanoparticles and 1-DNA molecules. We can achieve stable trapping of particles as small as 75nm, representing

some of the smallest dielectric matter ever trapped or transported using such a system. In addition to the experimental results, we also present an examination of the effect that the presence of a particle has on the optical mode, details of the trap strength and stiffness in comparison with other techniques, and a unique stability analysis descriptive of the release kinetics for particles near the stability point.

As shown in Figure 2.2a, we are able to capture and stably trap polystyrene nanoparticles (refractive index $n = 1.45$) with diameters of 75 nm and 100 nm in slot waveguides with widths of 100 nm and 120 nm, respectively. In all cases the optical power at the exit of the fibre used to couple light into the waveguide was less than 300 mW, the excitation wavelength was $\lambda = 1,550$ nm, and the trapping used TE polarization. Figure 2.2a illustrates our ability to capture and accumulate flowing particles in the slot waveguide for indefinite periods of time and release them by either reducing the optical power or switching the polarization. Excitation of the slot waveguides using transverse-magnetic (TM) polarization required three to five times as much power to obtain stable trapping, so switching polarization also tended to break the trap. The microfluidic flow serves to transport the particles to the waveguide but does not have a role in the trapping itself. This is indicated by the fact that the trap breaks on removal of the optical excitation in the above experiments.

Figure 2.2a also illustrates the dynamics of the capture of flowing particles in a trap near the stability point, where the random thermal energy in the system is of the same order as the amount of work required to break the trap [26]. The average retention time in such a trap is a statistical process governed by the release kinetics of the system, which in turn is governed by the trap strength, its stiffness and the location on the waveguide where the particle is trapped (as will be described below). In the

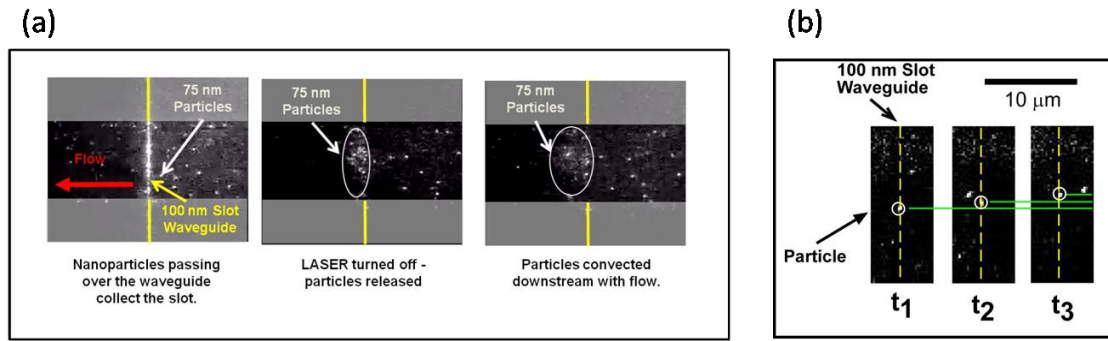


Figure 2.2: Trapping and transport of dielectric nanoparticles in a slot waveguide. **a**, Waveguide is optically excited while 75-nm polystyrene nanoparticles flow in the overlying microchannel over 100-nm slot waveguides. Over time, particles collect in the slot and also on the sides of the waveguide. At $t = 0$, the laser source is removed and particles are released from the waveguide. Immediately after release, a ‘cloud’ of particles forms as the particles leave their trapping sites and the released particles are carried down the channel by the fluid flow. **b**, Trapped 100-nm nanoparticles in 120-nm slot waveguides are transported a short distance by radiation pressure. Time-lapse images are cropped from images taken using a SensiCam CCD camera with contrast and brightness adjustments to the entire image. The cropping location is the same in each time-lapse image.

experiment shown, the nanoparticles are flowing by in the microchannel at an average speed of $80 \mu\text{m s}^{-1}$ and, as can be seen, the number of particles that are captured is low (less than 25%) in comparison with those that flow by. The reason for the low capture rate is that to be trapped, a particle must be on a streamline that passes through the evanescent field. This is analogous to a situation in which a flowing particle must pass through the focal point of a free-space optical tweezer in order to be trapped, and is not an inherent limitation of our system. The capture rate can be increased by decreasing the channel size, reducing the flow rate or increasing the optical power.

As mentioned above, an advantage of this approach is the ability not only to capture nanoscopic matter but to transport it optically. This capability is important for the development of active nanoassembly techniques and for optically driven bioanalytics [27]. From Rayleigh theory it is well known that the radiation-pressure-based transport

velocity of a dielectric nanoparticle is proportional to the local intensity and scales with the fifth power of particle radius [28]. As such it is extremely difficult to optically transport very small matter unless very high optical intensities can be achieved. As shown in Figure 2b, using our slot waveguide system we have been able to demonstrate optical propulsion of 100-nm particles at an average speed of $1.5 \mu\text{m/s}$ (using 250 mW optical power measured at the exit of the fibre). Because the

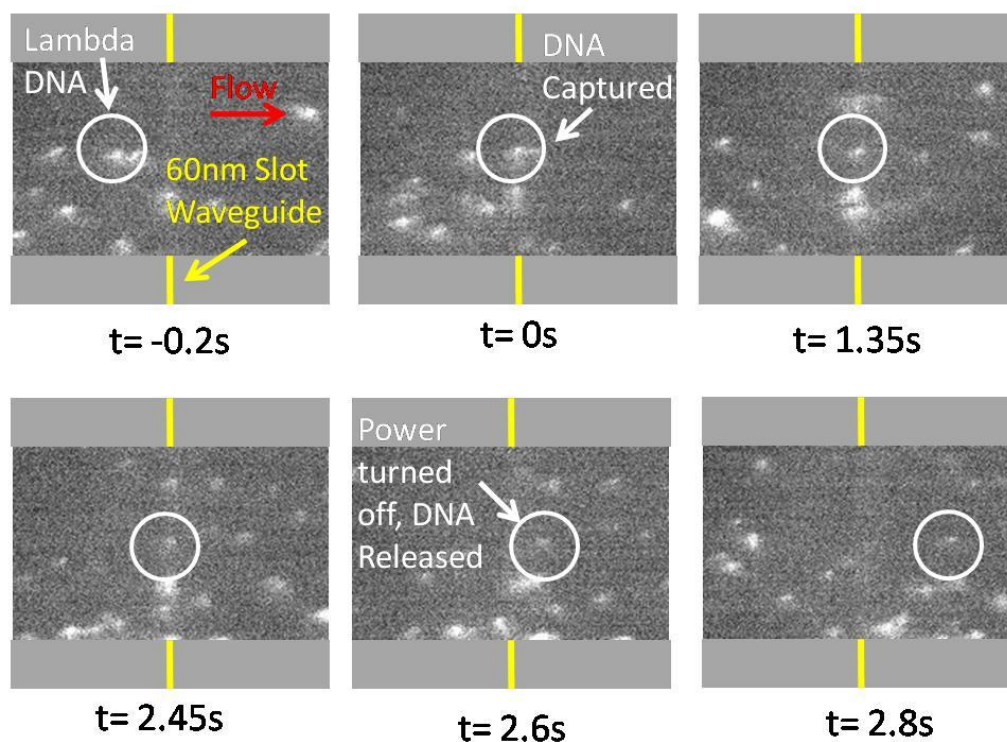


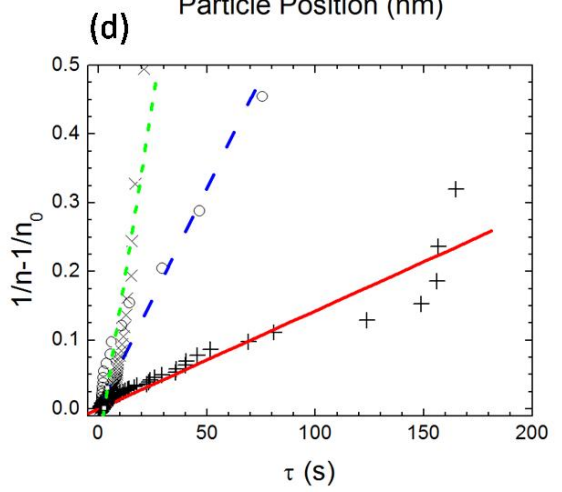
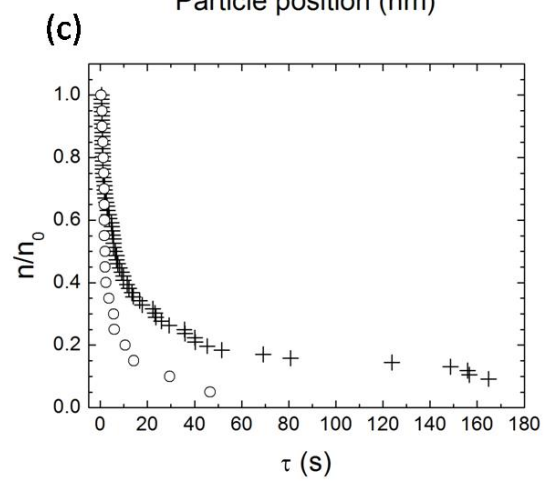
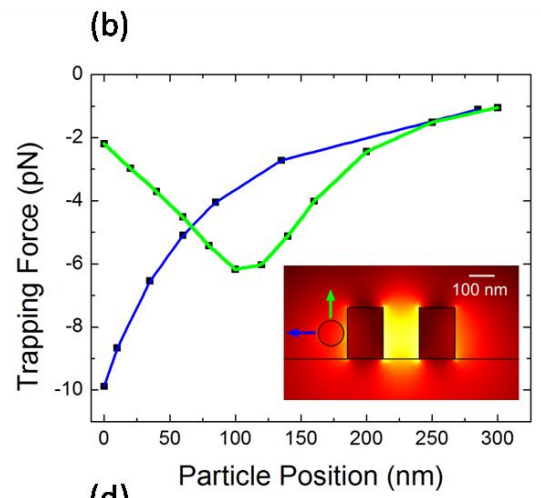
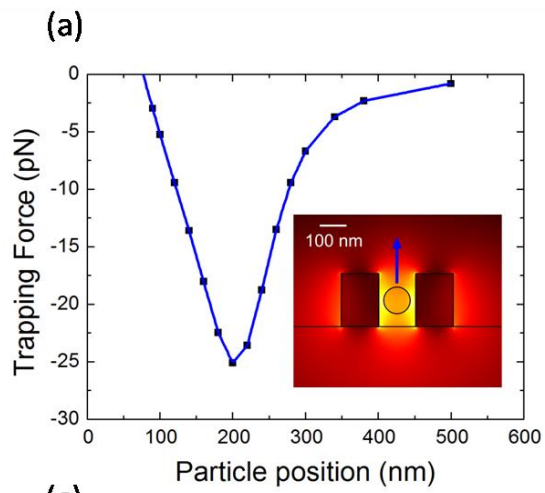
Figure 2.3: Capture and trapping of λ -DNA. Images show individual YOYO-tagged 48-kilobase λ -DNA flowing over an optically excited 60-nm-wide slot waveguide. At time $t = 0$ the encircled DNA is trapped. In this case the DNA is released at the 2.6-s mark and flows downstream. This shows the collection of DNA molecules over time and their release in response to removal of the optical excitation. Trapping conditions are identical to those used for the nanoparticle experiments shown in Figure 2. Time-lapse images are cropped from images taken using a SensiCam CCD camera with contrast and brightness adjustments to the entire image. The cropping location is the same in each time-lapse image.

propulsion velocity is inversely proportional to the fourth power of wavelength, one method by which the transport velocity could be increased is by using a different high-refractive-index material that is transparent at lower wavelengths.

Nanoscale dielectric particles can be considered as coarse approximate models for biological species such as viruses and very small bacteria. Of perhaps greater interest is the ability to capture and optically confine individual biomolecules. As shown in Figure 3, we have been able to capture from solution and stably trap individual strands of YOYO-1 tagged l-DNA molecules 48 kilobases long. As in previous cases, trapping was accomplished using 250 mW of input optical power at a wavelength of 1,550 nm; in this case, however, we used a 60-nm slot waveguide. As can be seen, when the power is removed the DNA strands are released. These experiments were done under pH conditions in which the DNA is reported to be in a partially extended state [7]. Although others have demonstrated optical trapping of l-DNA at pH levels at which the molecule is known to be in a supercoiled state [7, 8], it has proved difficult to trap partially extended molecules because the focal point of a tightly focused tweezer can only interrogate a small portion of the molecule. The slot waveguide technique allows us to trap extended molecules, as the confinement force is equivalently applied along a line rather than at a point. Further development of the transport technique may also allow us to develop new biomolecular separation mechanisms or new methods of interrogating single molecules for rapid sequencing [29] or direct haplotyping [30].

To characterize the trapping stability, stiffness and release kinetics better, we have carried out a detailed three-dimensional numerical analysis of the system. Referring back to Figure 2, although most of the particles were observed to be trapped in the high intensity slot region, trapping was also observed along the sides of the slot

Figure 2.4: Trapping forces on particles trapped inside and outside the slot waveguide, and analysis of particle release kinetics. The work required to release a particle from the trap is found by integrating the force curves from a particle’s stable trapping position to infinity. Inset images show the calculated electric field distribution with the particle in the two stable trapping positions. The arrows indicate the direction of release. **a**, Trapping force for a 100-nm particle in a 120-nm slot plotted against its position relative to the height of the slot waveguide. The particle position is measured as the distance of the particle centre from the bottom of the 200-nm-tall slot waveguide. The trapping force reaches a maximum at the point where the field gradient is strongest at the entrance to the slot waveguide. **b**, Trapping force for a 100-nm particle side-trapped in the same structure with two possible release paths. Particle position is measured as the deviation of the particle centre from its most stable position. The blue line corresponds to a particle being pushed off the waveguide due to an external force, and the green line corresponds to a particle being lifted up off the waveguide. The trapping forces listed are normalized to 1 W of guided power. **c**, Experimental data for N/N_0 plotted against normalized time, τ . Particles trapped in the slot are represented by crosses, side-trapped particles are represented by circles, and DNA by \times signs. The quantity N/N_0 represents the relative ‘concentration’ of particles trapped on the waveguide. **d**, Plot of $F(N)$ (see Supplementary Information) for a second-order rate law ($1/N - 1/N_0$) versus τ . The same symbols are used here as in **c**. The lines represent linear fits to the data from which the release rate constant can be obtained. In this case sharper slopes represent a higher release rate and therefore a less stable trap.



waveguide structure. Because the trap strength is related to the local optical field intensity, we can compare the behavior of particles trapped in the two different regions to gauge the effect on trapping stability. To do this, we used a finite-element simulation to calculate the relative trapping force for a side-trapped particle in comparison with one trapped in the slot, shown in Figure 4a, 4b. As can be seen, the trapping force for side-trapped particles is much smaller, and as a result less work energy is required to exceed the trapping release barrier. This provides an avenue to differentiate the two situations, as we would expect side-trapped particles to be released more easily than their slot trapped analogues. Figure 4a, 4b also illustrates that the optical mode of the slot waveguide is not greatly perturbed by the presence of the particle in either position.

Because the direction of trap release is in the vertical direction, and because of the physical confinement provided by the channel walls and the fact that the trapping force does not vary along the length of the waveguide, it is difficult to extract quantitative values for the trapping stability experimentally. From the numerical computations, however, we can estimate the trap stiffness from the slope of the force-distance curve as being 0.2 pN per nanometre for a 100-nm nanoparticle at 1-W excitation power. Although a direct comparison is difficult, this is significantly higher than previously described for larger particles using other near-field techniques (see Grigorenko *et al.* [4] who reported a 0.013 pN nm^{-1} stiffness for a 200-nm bead).

As described in previous analytical work [26], for a particle in an optical near field, there is a finite amount of work energy required to remove a particle from a stably trapped location to one where the trap no longer has any influence. When trapping is relatively weak and the particles small, the random thermal energy in the system will eventually exceed this work and the particle will be released. In such cases, the work

energy is analogous to an activation energy barrier that impedes the release of particles from the waveguide, and the kinetic behaviour is similar to molecular desorption from a surface (see Supplementary Information for the theoretical basis). Understanding how related parameters such as slot width, particle composition and particle size affect the release rate of trapped nanoparticles yields information necessary for the engineering of robust, stable slot transport devices.

We carried out a large number of trapping experiments for nanoparticles trapped inside the slot, nanoparticles trapped outside the slot, and the trapped DNA. Trapping was done near the stability point such that the targets would self-release from the waveguide structure. Figure 4c shows a plot of the total number of trapped targets on the waveguide as a function of normalized time. The average release time for particles trapped inside the slot is larger than that for those trapped outside, suggesting greater stability, consistent with our earlier numerical predictions. The trapping stability is related to a kinetic constant, k , which can be obtained by plotting the above data as a function of reduced time for an appropriate rate law (see Supplementary Information). In Figure 4d we see that side-trapped particles have a larger rate constant, suggesting that the release (desorption) is faster and a lower work energy is required for release. It is not yet clear why the release process seems to have a second-order rate, but we believe that it results from the exponential decay of the electromagnetic trapping force coupled with hydrodynamic drag. DNA shows a lower stability than the polystyrene nanoparticles, probably because of the extended conformation that it obtains during trapping. As the trapping stability is likely to be strongly dependent on molecular conformation, analysis of the release kinetics in such systems may result in a new method of single-molecule analysis.

Sub-wavelength slot waveguides such as those used in this work can be integrated into lab-on-a-chip platforms using existing manufacturing techniques. They allow discrete optical manipulation and transport of nanoscopic objects with greater precision than is available with existing approaches. The fusion of nanofluidics and optical manipulation in this manner could lead to new methods of bioanalysis and directed assembly.

2.1 Method Summary

We fabricate the slot waveguide chips using electron beam lithography. After experimental use, the chips are cleaned using Nanostrip, and scum is removed by using a reactive ion oxygen plasma etching process. The total width of the waveguides is 450 nm with slot widths ranging from 60 nm to 120 nm. The slot waveguides are transitioned to nanotaper devices clad in silicon oxide to increase the coupling efficiency. The laser source is a tunable 1,550-nm laser that runs to a tapered lensed fibre, using the same set-up previously used for our SU-8 waveguide experiments [21].

The particle solution consists of suspended fluorescent polystyrene nanoparticles 75 nm and 100 nm in diameter (Duke Scientific) with refractive index $n = 1.574$ in a 100 mM phosphate buffer solution. The particles have a dispersity in diameter of about 10%. The high ionic concentration of the buffer solution suppresses electrostatic interactions in the system and maintains a constant pH during experiments. We add 1%-by-volume Triton X-100 non-ionic surfactant to the particle solution to prevent aggregation of the nanoparticles and to limit adhesion of particles to the surface of the devices and PDMS microchannels.

The experiments use devices that are bonded to a PDMS microchannel 100 μm wide and 5 μm tall. The fluidics are driven using an adjustable airpressure system designed to maintain a constant pressure to the device. The power output of the fibre during the trapping experiments was set from 250 to 300 mW. Particle trapping was confirmed by counting immobilized particles and counting the number of released particles. We determined particle velocity measurements and particle trapping times by using the ImageJ particle tracking software. Images of the experiments were captured at a rate of 55 ms per frame using a SensiCam CCD camera.

As mentioned in the main text, we carried out experiments demonstrating l-DNA trapping using the technique described above, with the exception of the smaller 60-nm-wide slot waveguide. The l-DNA molecules (New England BioLabs) were stained with YOYO-1 intercalating dye (Molecular Probes) so that they could be observed using traditional fluorescence microscopy. The buffer consisted of 10mM Tris Base (J.T. Baker), 1mM EDTA (Fisher), and 10mM sodium chloride (Mallinckrodt) at a pH of 7.8. Poly(n-vinylpyrrolidone) (PVP, Sigma) 2% (by weight) was added to reduce unspecific binding of DNA to channel walls.

2.2 Supplemental Material: Kinetic Analysis of Trapping Stability

In the article, we stipulated that the amount of work required to release a trapped particle from the slot waveguide is directly related to the amount of force applied to the particle as it leaves the trapping region. This work energy required to release the particle can be thought of as an activation energy barrier to the particles release, an analogy to traditional molecular desorption theories. As a result, it is possible to characterize the rate constant for such a release mechanism using an Arrhenius law for a single particle system:

$$k = A \exp\left(-\frac{W_{trap}}{k_B T}\right) \quad (2.1)$$

where k is the particle release rate constant, A is the Arrhenius constant, W_{trap} is the work required to release a particle from a slot waveguide, k_b is Boltzmann's constant, and T is the temperature of the system. It has been shown that W_{trap} scales linearly with the optical intensity in a waveguide, so we can write:

$$\bar{k} = k_0 \exp\left(\frac{P}{P_0} \frac{A_0}{A}\right) \quad (2.2)$$

where k_0 represents a baseline rate constant, P is the optical power coupled in the waveguide, P_0 is a baseline power, A is the cross-sectional area of the slot, and A_0 is a baseline area. The rate at which particles release can be written using a rate law:

$$\frac{dn}{dt} = -kn^x \quad (2.3)$$

where n is the number of particles trapped and x is a whole number representing the order of the desorption process. The solution of the differential equation would be of the form:

$$F(n) = k_0 \tau \quad (2.4)$$

$$\tau = \exp\left(\frac{P}{P_0} \frac{A_0}{A}\right) t \quad (2.5)$$

where $F(n)$ is some function of n and τ is an intensity normalized time. The equations above are similar to the Polanyi-Wigner [31] equations for gas desorption from a surface, but written here for the desorption of single particles as opposed to large numbers of gas molecules. This assumption is only valid for the case where the

surface coverage of the total number of particles is relatively small such that they don't interfere with one another.

REFERENCES

- [1] D. G. Grier, "A revolution in optical manipulation," *Nature*, **424**, 810-816, (2003).
- [2] A. Ashkin, J. M. Dziedzic, J. E. Bjorkholm, and S. Chu, "Observation of a Single-Beam Gradient Force Optical Trap for Dielectric Particles," *Optics Letters*, **11**, 288-290, (1986).
- [3] M. P. MacDonald, G. C. Spalding, and K. Dholakia, "Microfluidic sorting in an optical lattice," *Nature*, **426**, 421-424, (2003).
- [4] A. N. Grigorenko, N. W. Roberts, M. R. Dickinson, and Y. Zhang, "Nanometric optical tweezers based on nanostructured substrates," *Nature Photonics*, **2**, 365-370, (2008).
- [5] M. Born and E. Wolf, *Principles of optics : electromagnetic theory of propagation, interference and diffraction of light*, 6th ed. Oxford ; New York: Pergamon Press, 1980.
- [6] V. R. Almeida, Q. F. Xu, C. A. Barrios, and M. Lipson, "Guiding and confining light in void nanostructure," *Optics Letters*, **29**, 1209-1211, (2004).
- [7] D. T. Chiu and R. N. Zare, "Biased diffusion, optical trapping, and manipulation of single molecules in solution," *Journal of the American Chemical Society*, **118**, 6512-6513, (1996).
- [8] K. Hirano, H. Nagata, T. Ishido, Y. Tanaka, Y. Baba, and M. Ishikawa, "Sizing of single globular DNA molecules by using a circular acceleration technique with laser trapping," *Analytical Chemistry*, **80**, 5197-5202, (2008).
- [9] D. Psaltis, S. R. Quake, and C. H. Yang, "Developing optofluidic technology through the fusion of microfluidics and optics," *Nature*, **442**, 381-386, (2006).
- [10] C. Monat, P. Domachuk, and B. J. Eggleton, "Integrated optofluidics: A new river of light," *Nature Photonics*, **1**, 106-114, (2007).
- [11] S. L. Neale, M. P. Macdonald, K. Dholakia, and T. F. Krauss, "All-optical control of microfluidic components using form birefringence," *Nature Materials*, **4**, 530-533, (2005).

- [12] P. Y. Chiou, A. T. Ohta, and M. C. Wu, "Massively parallel manipulation of single cells and microparticles using optical images," *Nature*, **436**, 370-372, (2005).
- [13] G. L. Liu, J. Kim, Y. Lu, and L. P. Lee, "Optofluidic control using photothermal nanoparticles," *Nature Materials*, **5**, 27-32, (2006).
- [14] M. M. Wang, E. Tu, D. E. Raymond, J. M. Yang, H. C. Zhang, N. Hagen, B. Dees, E. M. Mercer, A. H. Forster, I. Kariv, P. J. Marchand, and W. F. Butler, "Microfluidic sorting of mammalian cells by optical force switching," *Nature Biotechnology*, **23**, 83-87, (2005).
- [15] G. Sinclair, P. Jordan, J. Courtial, M. Padgett, J. Cooper, and Z. J. Laczik, "Assembly of 3-dimensional structures using programmable holographic optical tweezers," *Optics Express*, **12**, 5475-5480, (2004).
- [16] D. L. Andrews, *Structured light and its applications : an introduction to phase-structured beams and nanoscale optical forces*. Amsterdam ; Boston: Academic, 2008.
- [17] R. F. Marchington, M. Mazilu, S. Kuriakose, V. Garcés-Chávez, P. J. Reece, T. F. Krauss, M. Gu, and K. Dholakia, "Optical deflection and sorting of microparticles in a near-field optical geometry," *Opt. Express*, **16**, 3712-3726, (2008).
- [18] M. Righini, A. S. Zelenina, C. Girard, and R. Quidant, "Parallel and selective trapping in a patterned plasmonic landscape," *Nature Physics*, **3**, 477-480, (2007).
- [19] T. Cizmar, M. Siler, M. Sery, P. Zemanek, V. Garces-Chavez, and K. Dholakia, "Optical sorting and detection of submicrometer objects in a motional standing wave," *Physical Review B*, **74**, -, (2006).
- [20] L. N. Ng, B. J. Luf, M. N. Zervas, and J. S. Wilkinson, "Forces on a Rayleigh particle in the cover region of a planar waveguide," *Journal of Lightwave Technology*, **18**, 388-400, (2000).
- [21] B. S. Schmidt, A. H. Yang, D. Erickson, and M. Lipson, "Optofluidic trapping and transport on solid core waveguides within a microfluidic device," *Opt. Express*, **15**, 14322-14334, (2007).

- [22] K. Grujic, O. G. Helleso, J. P. Hole, and J. S. Wilkinson, "Sorting of polystyrene microspheres using a Y-branched optical waveguide," *Optics Express*, **13**, 1-7, (2005).
- [23] S. Gaugiran, S. Getin, J. M. Fedeli, and J. Derouard, "Polarization and particle size dependence of radiative forces on small metallic particles in evanescent optical fields. Evidences for either repulsive or attractive gradient forces," *Optics Express*, **15**, 8146-8156, (2007).
- [24] L. N. Ng, B. J. Luff, M. N. Zervas, and J. S. Wilkinson, "Propulsion of gold nanoparticles on optical waveguides," *Optics Communications*, **208**, 117-124, (2002).
- [25] S. Gaugiran, S. Getin, J. M. Fedeli, G. Colas, A. Fuchs, F. Chatelain, and J. Derouard, "Optical manipulation of microparticles and cells on silicon nitride waveguides," *Optics Express*, **13**, 6956-6963, (2005).
- [26] A. H. J. Yang and D. Erickson, "Stability analysis of optofluidic transport on solid-core waveguiding structures," *Nanotechnology*, **19**, 045704, (2008).
- [27] S. J. Hart, A. Terray, T. A. Leski, J. Arnold, and R. Stroud, "Discovery of a significant optical chromatographic difference between spores of *Bacillus anthracis* and its close relative, *Bacillus thuringiensis*," *Analytical Chemistry*, **78**, 3221-3225, (2006).
- [28] K. Svoboda and S. M. Block, "Optical Trapping of Metallic Rayleigh Particles," *Optics Letters*, **19**, 930-932, (1994).
- [29] I. Braslavsky, B. Hebert, E. Kartalov, and S. R. Quake, "Sequence information can be obtained from single DNA molecules," *Proceedings of the National Academy of Sciences of the United States of America*, **100**, 3960-3964, (2003).
- [30] A. T. Woolley, C. Guillemette, C. L. Cheung, D. E. Housman, and C. M. Lieber, "Direct haplotyping of kilobase-size DNA using carbon nanotube probes," *Nature Biotechnology*, **18**, 760-763, (2000).
- [31] K. Kolasinski, *Surface Science: Foundations of Catalysis and Nanoscience*. West Sussex, England: John Wiley & Sons Ltd, 2002.

3.0 Forces and Transport Velocities for a Particle in a Slotted Waveguide*

Optofluidic transport seeks to exploit the high-intensity electromagnetic energy in waveguiding structures to manipulate nanoscopic matter using radiation pressure and optical trapping forces. In this paper, we present an analysis of optical trapping and transport of sub-100 nm polystyrene and gold nanoparticles in silicon slot waveguides. This study focuses on the effect of particle size, particle refractive index, and slot waveguide geometry on trapping stability and the resulting transport speed. Our results indicate that stable trapping and transport can be achieved for objects as small as 10 or 20 nm in diameter with as much as a 100 fold enhancement in trapping stiffness over the state of the art.

3.1 Introduction

The field of optofluidics [1, 2] focuses on the integration of microfluidic devices with photonic [3] components. Prominent examples of such integration include: liquid core ARROW waveguides [4], hydrodynamically tunable optofluidic lenses [5], particle manipulations using opto-electronic tweezers [6] and photothermally driven microfluidic transport [7]. Recently there has been an increased focus in optofluidics as it relates to optical manipulation of micro and nanoparticles in fluidic environments [8-10]. For example, the optical tweezer [11] has been used to manipulate and trap microscale objects [12], liquid droplets [13] and even some sub-micron objects such as

* This chapter was previously published in A. H. J. Yang, T. Lertsuchatawanich, and D. Erickson, "Forces and Transport Velocities for a Particle in a Slot Waveguide," *Nano Letters*, **9**, 1182-1188, (2009). Reproduced with permission from the American Chemical Society.

viruses [14] and silver nanoparticles [15]. The advantages of optical manipulation include the precision and parallel nature with which matter can be handled and the relatively simple integration of free space optics with chip-based microfluidic devices. Ultimately however, optical tweezers are fundamentally limited by the natural diffraction of light. Firstly the diffraction limit places an upper bound on how tightly a laser can be focused and by extension the trapping force which can be generated. Secondly due to the well known relationship between spot size and depth of focus, there is a tradeoff between increased focus versus the available interaction length. As such, long distance optical transport of nanoscopic matter using freespace light is very difficult.

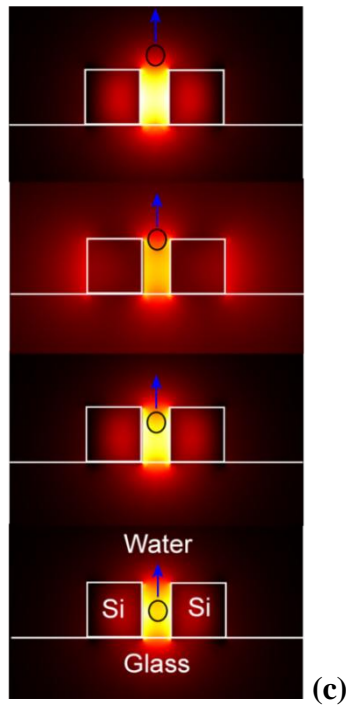
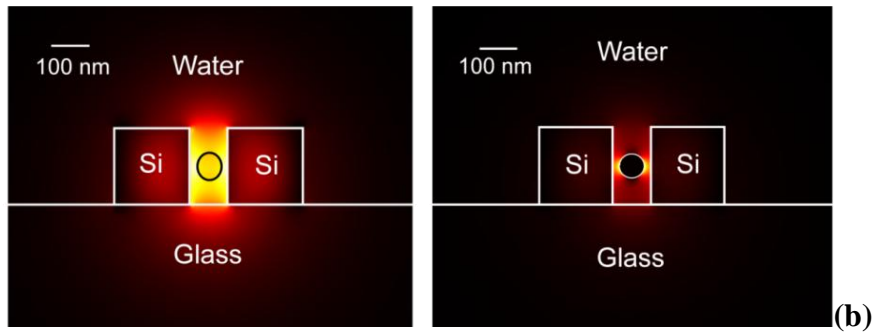
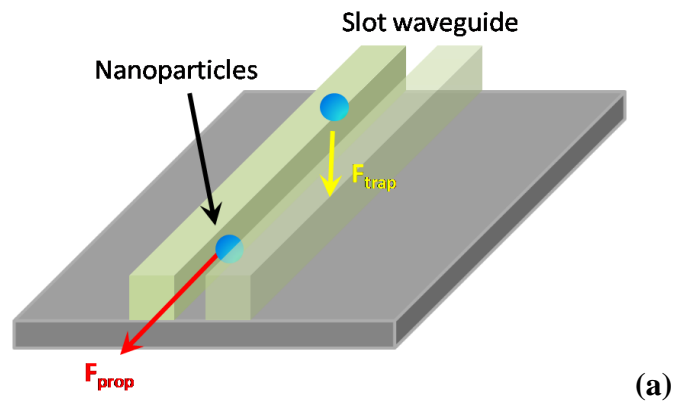
One solution to the diffraction limit challenge is in using optical waveguides to confine light within solid structures [16]. Light confined in such a manner is considered a self-consistent wave and can propagate through a waveguide indefinitely without losses or changing its form. As a result of this unique feature, objects in the optical field of a waveguide can be propelled via radiation pressure along the length of a waveguide for an indefinite distance (not limited by the depth of focus of a laser focus). Solid-core waveguides have been shown to be able to transport a variety of objects such as cells [17], gold nanoparticles [18], and sub-micron polystyrene beads via evanescent field interactions [19]. Previously, Yang and Erickson [20] proposed a numerical finite-element method for studying the trapping stability of sub-micron particles trapped on solid core waveguides. More recent experimental work has focused on improving the efficiency of waveguides for trapping and transport, with efforts in creating hollow-core^[4] and liquid-core [21] waveguides, which allow access to the entire optical mode.

Recently Yang *et al.* [22] demonstrated the trapping and transport of polystyrene nanoparticles and DNA molecules using slotted silicon waveguides. The slot waveguide, shown in Figure 1(a), is comprised of a nanoscale region of low refractive index flanked by two materials of drastically higher refractive index. The high index contrast in the slot region creates a pseudo transverse-electric mode which exhibits large electric field discontinuities at the slot-waveguide boundaries. The effect of the small slot size and the large field discontinuities at the high/low index boundaries generates a high-intensity eigenmode in the slot, such that the majority of the optical energy is confined within the accessible low-index region. The advantage of such a technique is in confining light in the slot cavity of the waveguide, allowing combined hollow-core and liquid-core behavior and creating strong optical intensities and gradients.

In this paper we examine theoretically the optical trapping and transport of nanoparticles of different composition, namely polystyrene and gold in these silicon slotted waveguides. This study comprises of numerical simulation and analysis of trapping stability and transport velocities for a range of applicable experimental parameters. Our goal here is to discern the fundamental limits of this method of nanoscale transport. This study focuses on the effect of particle size, particle refractive index, and slot waveguide geometry on trapping stability and the resulting transport speed.

Figure 3.1(a) illustrates the slotted waveguide model system used in this study. The waveguide structure itself is fabricated from silicon on a glass substrate. Analogous to the experimental system presented in Yang *et al.* [22], a microfluidic channel runs over the slot waveguide transporting particles to the trap. The upper cladding therefore has the properties of water and the lower cladding the properties of silicon

Figure 3.1: Nanophotonic Optofluidic Transport. (a) Schematic of forces acting on nanoparticles in a slot waveguide. (b) Simulation images comparing optical intensity of 65 nm polystyrene and gold nanoparticles in a 100 nm slot waveguide. (c) Compilation of images showing a 65 nm polystyrene nanoparticle as it moves up and out of a slot waveguide.



dioxide. The slot region of the waveguide is exposed to the region directly above it, which allows suspended nanoparticles to directly access light propagating through the waveguide. Table 3.1 below summarizes the refractive index and geometric properties used in our simulations. 1550 nm light was used here because of the relative transparency of all the materials in the system at that wavelength. We choose to analyze polystyrene particles here because they have a low absorption cross-section and low index contrast relative to water based environments. In addition, these particles coarsely mimic the properties of organic and biological materials. We also examine the use of gold nanoparticles because of their high absorption cross section and refractive index contrast properties.

Table 3.1: Simulation and Geometric Parameters

Domain	Material	Domain size ^a	Refractive index
Waveguide	Silicon	200 x 200 nm (each)	3.48
Slot width	Water	100 nm/40 nm	1.33
Substrate	Silicon dioxide	Lower subdomain	1.45
Microfluidic channel	Water	Indefinite	1.33
Particle A	Polystyrene	10 – 65 nm	1.55
Particle B	Gold	10 – 65 nm	0.18+10.21 <i>i</i>

^a Waveguide dimensions given as cross-section

In our previous work [20], we demonstrated that the primary driving force behind trapping stability is that there is a finite work energy required to remove a particle from a stably trapped location to one where the trap no longer has any influence. To summarize:

$$S = \frac{W_{\text{trap}}}{k_{\text{B}}T} \quad (3.1)$$

where S is the stability number, W_{trap} is the work energy required to remove a particle from a trap, k_{B} is the Boltzmann constant, and T is the system temperature. The Boltzmann term, $k_{\text{B}}T$ is used to represent the random thermal energy of the particle due to Brownian motion. As particle size decreases from micrometer to nanometer dimensions, $k_{\text{B}}T$ comprises a relatively larger portion of total energy imparted to the particle, resulting in stronger thermal motion. The stability number, S , can be used to describe the relative strength of an optical trap against such random motion and other external forces, where higher numbers representing stronger traps. For a trap that has a single direction of release, the work can be described as the integral of the forces exerted on the particle as it moves in the direction of release. The electromagnetic force acting on the particle can be described using

$$W_{\text{trap}} = \int F_{\text{trap}} dx \quad (3.2)$$

$$(3.3)$$

where F_{trap} is the trapping force, $\langle \mathbf{T}_M \rangle$ is the time averaged Maxwell Stress Tensor (MST), and \mathbf{n} is the normal vector. Interested readers are directed to Yang and Erickson [20] for more information on electromagnetic forces. Furthermore, equation 1 can be used to relate the energy of the trap to a kinetic release rate. We can characterize the rate constant for such a release mechanism using an Arrhenius law:

$$k = A \exp\left(-\frac{W_{\text{trap}}}{k_{\text{B}}T}\right) = A \exp(-S) \quad (3.4)$$

where k is the particle release rate constant, A is the Arrhenius constant, k_{B} is Boltzmann's constant, and T is the temperature of the system. Equation 4 can be used as part of a rate law in order to define a relationship between the rate of release of

nanoparticles from a slot waveguide trap and the overall strength of the trapping potential. Interested readers are directed to McCann *et al.* [23] or Kolasinski [24] for more detailed information regarding nanoparticle escape from trapping potentials.

We can also find the steady state velocity for a particle in a slot waveguide by equating the propulsion forces (\mathbf{F}_{prop}) with the hydrodynamic drag force (\mathbf{F}_{Drag}).

$$\mathbf{F}_{\text{Prop}} = \mathbf{F}_{\text{Drag}} \quad (3.5)$$

$$\mathbf{F}_{\text{Drag}} = C_{\text{Drag}} \mathbf{U} \quad (3.6)$$

$$\mathbf{U} = \frac{\mathbf{F}_{\text{Prop}}}{C_{\text{Drag}}} \quad (3.7)$$

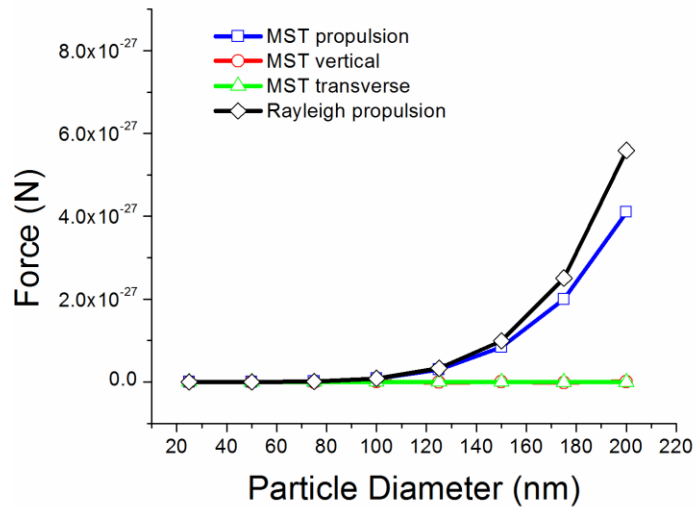
where \mathbf{F}_{Prop} is the force of scattered and absorbed photons on a particle, \mathbf{F}_{Drag} is the hydrodynamic drag on a particle, C_{Drag} is the drag coefficient of the particle, and \mathbf{U} is the steady state velocity. For the case of a sphere moving through a stagnant fluid, C_{Drag} is the Stokes drag coefficient $6\pi\eta a$, where η is the fluid viscosity and a is the particle radius. For a particle close to a surface, a near wall correction can be added to account for close proximity to a flat surface [25]. The most accurate method, which is used in our analysis, is through simulation of the particle/geometry domain and determining C_{Drag} numerically. To determine this here all parallel boundaries surrounding the nanoparticle are assigned a negative slip velocity to simulate the movement of a nanoparticle through the slot waveguide. Given the slip velocity and \mathbf{F}_{Drag} from this simulation C_{Drag} can be computed from Eq. 3.7.

Numerical calculations were conducted using a finite-element method. Geometric parameters for the simulations used in our case studies are listed in Table 1. Here we outline our methods for calculating the steady-state electric and velocity fields and the determination of the optical forces and hydrodynamic drag on spherical nanoparticles

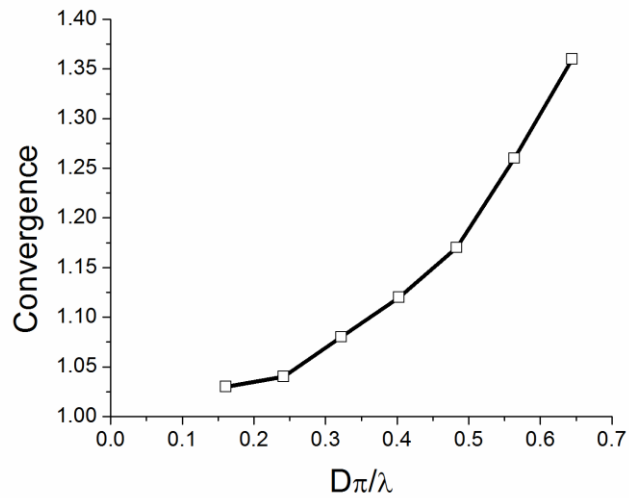
in slotted waveguides, along with our key assumptions. The electromagnetic field distribution in a slotted waveguide is determined by solving Maxwell's equations for the waveguide geometry, including the upper and lower cladding regions. A perfectly matched layer (PML) region is added to the output boundary of the geometry to absorb incoming radiation with minimal reflection. The input field distribution is determined by the solution of a boundary mode eigenvalue solver. The surrounding boundaries allow for a non-zero flux of scattered light, as expected for an unbounded cladding region. We determine the steady-state velocity field through the solution of the Stokes' equations, assuming incompressible flow and a viscous flow, which characterizes low Reynolds number flow in a microchannel. The input and output boundaries enforce a zero normal stress condition.

In our simulations, we assume that the relevant electromagnetic and hydrodynamic equations can be decoupled, and thus the optical and drag forces can be computed independently of each other. We do not consider the effect of absorption of light at 1550 nm by the water surrounding the waveguide. In an experimental system, however, the maximum power available would be limited by the amount of heat that is absorbed. One method for dealing with high water absorption is in using deuterium oxide (heavy water) for the fluid medium, which has a significantly lower absorption at 1550 nm [26]. We also neglect the effects of electrical double layer (EDL) repulsion. We do state that an aqueous solution at an ionic strength of 100 mM would have a characteristic repulsion range of approximately 1 nm, which is smaller than the length scales involved in our model.

Numerical validation (experimental validation is provided below) of the finite element simulation method was accomplished by creating a simulation that would mimic the conditions of a uniform plane wave incident on a nanoparticle. The simulation



(a)



(b)

Figure 3.2: Comparison of Maxwell Stress Tensor (MST) to Rayleigh scattering. (a) Plot of simulated optical force due to a plane wave incident on a particle and calculated forces using the Rayleigh scattering equation for increasing particle sizes. (b) Plot of convergence ($1 - F_{\text{MST}}/F_{\text{Ray}}$) versus the Rayleigh criterion ($D\pi/\lambda$).

domain consists of a cube containing liquid water, with a dielectric nanoparticle suspended in the center of the cube. Surrounding the box region are perfectly matched layer PML boundaries designed to absorb all scattered and incident light. Using this geometry, we simulated the effects of a plane wave as it scatters off the nanoparticle, and the scattering force on the nanoparticle. Shown in Figure 3.2, we plot the results of these simulations against calculated results using the Rayleigh scattering equation, changing only the particle diameter in subsequent iterations. As expected, we note that there is an insignificant amount of force generated in directions orthogonal to optical propagation. However, for particles above 100 nm in diameter, deviations appear in simulated values compared to Rayleigh theory. Shown in Figure 3.2(b), plotting the convergence between simulated and calculated values versus the Rayleigh criterion ($D\pi/\lambda \ll 1$), where D is the particle diameter, and λ is the freespace wavelength, we see that as $D\pi/\lambda$ gets larger, convergence between the two methods decreases. This agrees with similar calculations conducted for particle propulsion on silicon nitride waveguides [27] and our previous work [19, 20] that observed size dependences much lower than the predicted 6th order and 3rd order dependencies for Rayleigh scattering and gradient forces.

3.2 Results and Discussion

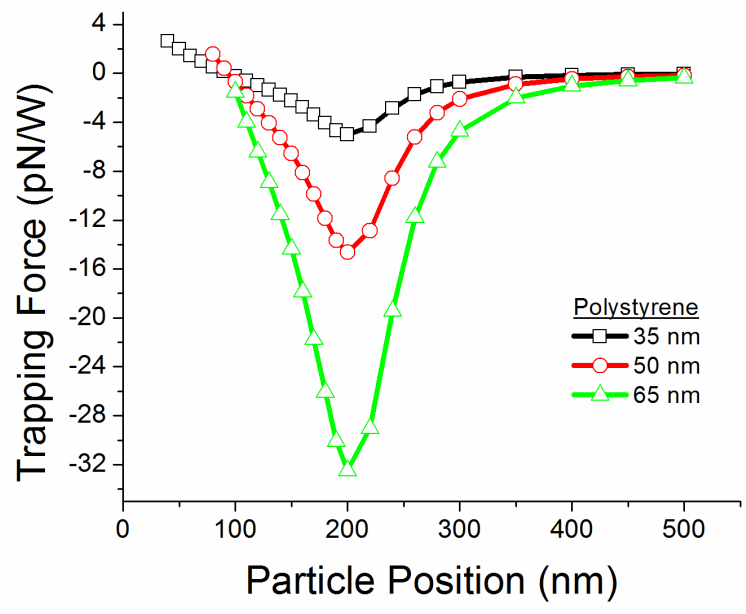
As stated previously, in this study we seek to determine practical limits for nanophotonic optofluidic transport. Figure 3.3 illustrates the trapping forces exerted on polystyrene and gold nanoparticles for varying vertical positions in the waveguide structure. Qualitatively, we note three key features of these force profiles. Particles that are positioned below the median of the waveguide structure (100 nm) tend to exhibit a net upward force, while particles positioned above the median point exhibit a net downward force. This suggests that the optical gradient in the waveguide tends to

guide particles toward the middle of the structure where the intensity is at its maximum. A second feature we observe is that the trapping force attains its maxima in all profiles at a height of 200 nm corresponding to the height of the waveguide. This point, as seen in Figure 3.3(c), represents the position at which the intensity gradient is at its largest, which agrees with theoretical predictions. Once the trapping force has reached its maxima, it decays rapidly to zero, which is representative of the fast decline of the evanescent wave behaving regions of the waveguide structure. The characteristic decay length of the force profiles appears to be on the order of 50 – 100 nm which is much shorter than previously reported results for particles on single mode waveguides.

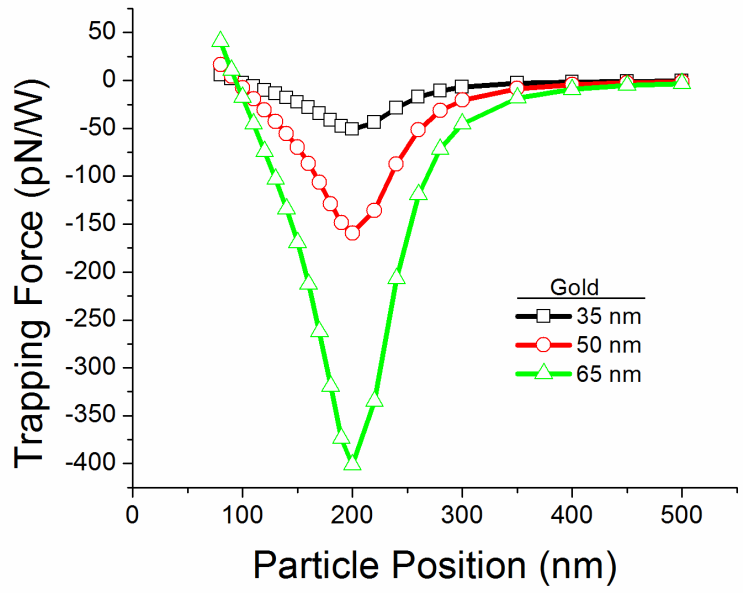
Several observations can be made regarding the sensitivity of the trapping force with respect to the variables of interest. As expected particles of increasing diameter experience stronger trapping forces in the slot waveguide. This sensitivity also is stronger than previously reported results for microspheres and larger sub-micrometer objects with similar refractive index [17, 20]. The increased dependence results from the much smaller nanoparticles used in this study which more closely approximate Rayleigh particles, and thus come closer to exhibiting the theoretical 3rd order sensitivity to particle size. The calculated force profiles for gold nanoparticles, shown in Figure 3.3(b) showed stronger trapping compared to polystyrene beads of the same size. This effect can be attributed to the relatively large refractive index contrast between water and gold.

Figure 3.4(a) shows the propulsion force profiles for gold particles in slot waveguides. We see similar dependences on size to those in Figure 3.3 with some differences. The size sensitivity of the propulsion force profiles is much more pronounced in comparison to the trapping force, power law fits of the average propulsion velocities

Figure 3.3: Trapping forces on nanoparticles in a 100 nm slot. Plots of trapping forces for particles at varying vertical position within the slot waveguide for (a) polystyrene nanoparticles and (b) gold nanoparticles.

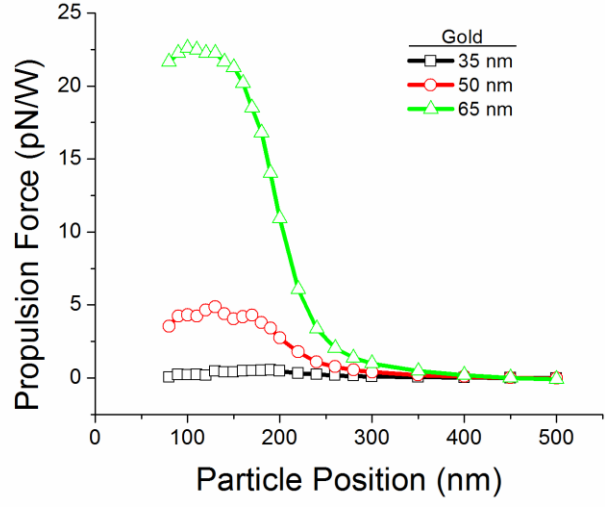


(a)

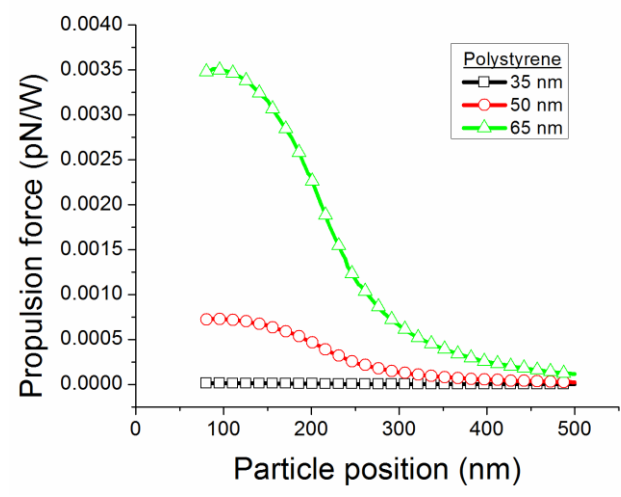


(b)

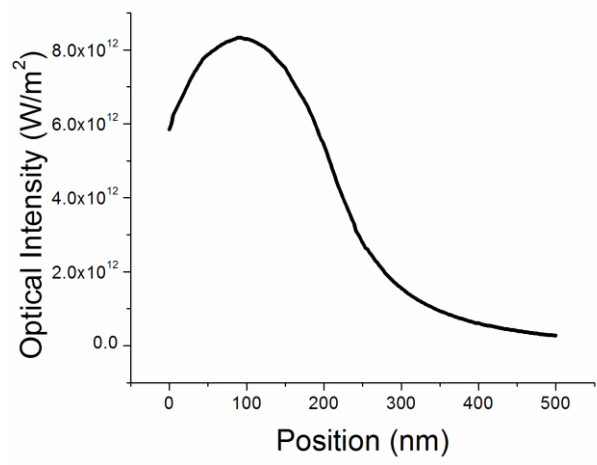
Figure 3.4: Propulsion forces on nanoparticles in a 100 nm slot. Plots of propulsion forces (in the direction of optical propagation) of particles at varying vertical positions within the slot waveguide for (a) gold nanoparticles and (b) polystyrene nanoparticles. The polystyrene propulsion force values were obtained by calculating the scattering force on the particles given the optical intensity profile within the waveguide assuming Rayleigh scattering. (c) Optical intensity in the waveguide as a function of the vertical position.



(a)



(b)

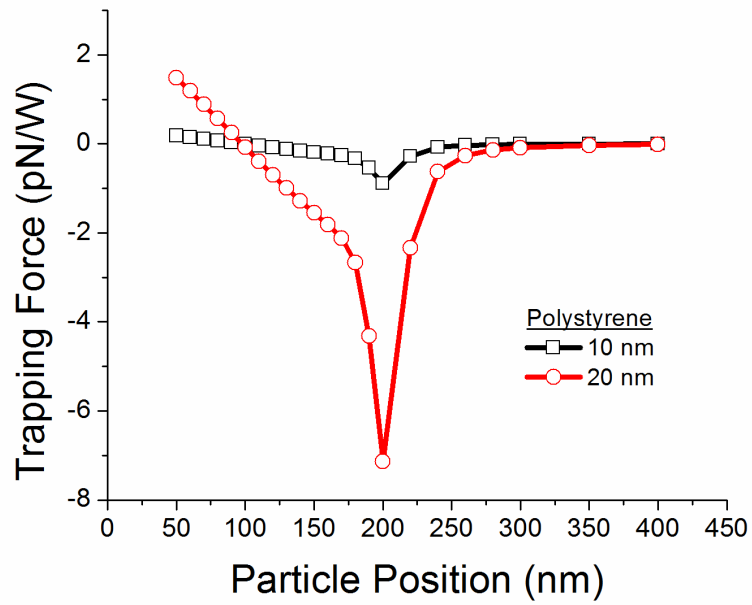


(c)

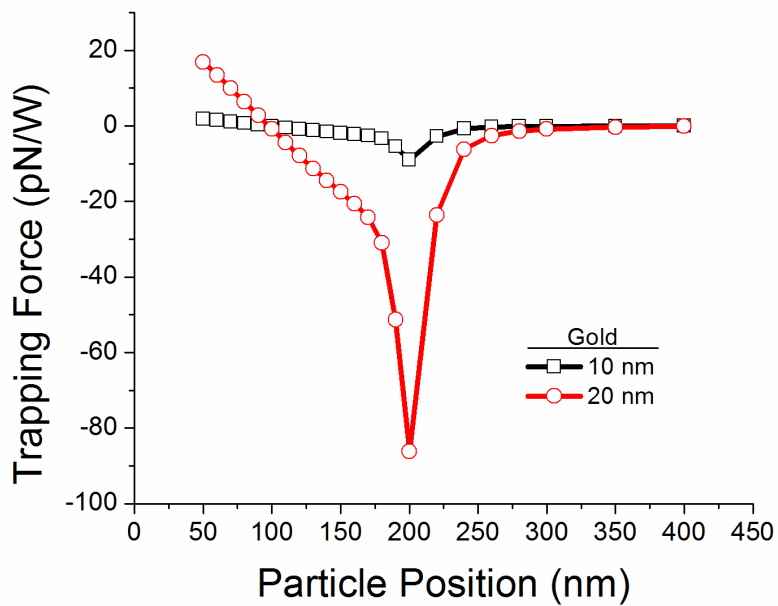
yield a 6th order relationship with respect to size, which is consistent with Rayleigh theory. Figure 3.4(c), which shows the optical intensity in a slot waveguide illustrates the strong proportionality between intensity and the propulsion forces exerted upon it, which is predicted by Rayleigh theory. Direct propulsion force values for polystyrene nanoparticles could not be obtained, because the values were several orders of magnitude below the numerical resolution. We can however extend the Rayleigh particle assumption to polystyrene particles (within the regime validated by the results presented in Figure 2), and calculate the scattering forces exerted upon them as shown in Figure 3.4(b). As expected we find that the propulsion forces exerted on a polystyrene particle is many orders of magnitude smaller than the gold nanoparticles.

There are also significant effects from decreasing slot width, resulting in an increase the optical intensity in the waveguide, shown in Figure 3.5. Unlike the trapping profiles for the larger nanoparticles (Figure 3.3), we notice a very sharp increase in the trapping force as the particle position approaches the lip of the slot waveguide. Simulations show that in the larger 100 nm slot, the calculated trapping forces for 10 and 20 nm particles are relatively small. However, in a 30 nm slot, the trapping forces increases to values approximate to those of larger nanoparticles in the 100 nm slot system. We also notice a very sharp increase in the trapping force as the particle position approaches the lip of the slot waveguide. As such increasing or decreasing the slot width is a controllable parameter that can variably tune the trapping force to more effectively target smaller or larger targets.

From the data provided from Figure 3.3 and Figure 3.4, we can calculate the stability numbers and steady state velocities using equations 3.1 and 3.6 described previously. These results are summarized in Table 3.2. Assuming ideal coupling, the threshold power outlines the required coupled power in a slotted waveguide in order to achieve a



(a)



(b)

Figure 3.5: Trapping force for nanoparticles in a 30 nm slot. Trapping forces exerted on nanoparticles in a 30 nm slot for (a) polystyrene nanoparticles and (b) gold nanoparticles.

stability number equal to 1, which is the minimum value of S required to trap a particle. Considering losses in experimental systems and that we do not consider any bulk fluid flow in our model, our predictions here underestimate the amount of power required for optical trapping in a slot waveguide. Even with these numbers, we observe trapping a 10 or 20 nm object with a refractive index contrast similar to or smaller than polystyrene would be near impossible due to the relatively large power requirements. However, because of the higher refractive index contrast between gold and water, we believe it is experimentally viable to trap colloidal gold particles in slotted waveguides with very small widths.

We also tabulate the calculated values of the trap stiffness, obtained by calculating the slope of the trapping force profile. Based on previously reported values for trapping stiffness in a plasmonic tweezer experiment of 0.013 pN/nm/W (upper limit value) [28] for 200 nm polystyrene particles, we predict our system has an enhancement of about 100x for particles of similar composition and size. Also, experimental results for the trapping of gold nanoparticles in optical tweezers reports trapping stiffness values approximately 100 times smaller than our predicted values using a slotted waveguide[29]. Table 3.2 also lists the calculated steady state velocities for the different sized particles. In this analysis, we use the values for average propulsion force and particle drag in the slot structure. Just as with the threshold power, these values here represent ideal values where coupling losses and losses in the waveguide would result in a loss of efficiency in the system. Within these limitations, we can see that for low refractive index contrast materials, optofluidic propulsion for objects below a diameter of 50 nm is very small due to the size sensitivity of the scattering force. Table 3.2 also lists the calculated steady state velocities for the smaller set of nanoparticles. In this analysis, we use the values for average propulsion force and

Table 3.2: Stability, trapping stiffness , and steady state velocities

particle material	diameter ^a (nm)	stability number (W ⁻¹)	threshold power (mW)	trap stiffness (pN/nm/W)	average velocity (μm/s/W)
Polystyrene	65	875	1.14	1.25	29.6
	50	392	2.55	0.556	9.81
	35	122	8.19	0.188	0.275
	20	140	7.14	0.131	-
	10	17.3	57.8	0.01624	-
Gold	65	9890	0.101	14.2	13800
	50	4120	0.243	5.82	4530
	35	1330	0.75	1.89	716
	20	1590	0.628	1.50	-
	10	174.2	5.74	0.164	-

^a Table values for 10 and 20 nm diameter particles were calculated using 30 nm slot width

particle drag in the slot structure. Just as with the threshold power, these values here represent ideal values where coupling losses and losses in the waveguide would result in a loss of efficiency in the system. With these limitations, optofluidic propulsion for objects with low refractive index contrast below a diameter of 50 nm is very small due to the size sensitivity of the scattering force.

Using data from experiments and the devices previously detailed in Yang *et al.* [22], we can compare our predicted values to experimental measurements of steady-state velocities of nanoparticles in slot waveguides in order to validate the above predictions. The average speed of the 100 nm diameter polystyrene spheres was found to be 2.3 ± 2.5 μm/s. In those experiments, an input power of 250 mW light at 1550 nm was used with a measured output of 1 mW. Assuming a -3 dB coupling loss, and a

uniform loss per unit distance over the length of the chip with the slot waveguide position about 3 mm from the edge of a 1 cm long waveguide, we estimate approximately 25 mW was coupled into the slot waveguides. Using the same methods described earlier to calculate the values in Table 3.2, but with modifications in the simulations to account for a 100 nm polystyrene bead in a 140 nm slot waveguide, we calculate the steady-state velocity to be 1.3 $\mu\text{m/s}$ at 25 mW of guided power which is of the same order as that predicted by our model. The discrepancy between the two results is most likely due to the inability to get an accurate measure of the actual power at the slot location in the experiments and the relatively large spread in the observed transport velocities

In conclusion, we have shown through our analysis and simulation results that the trapping and transport of nanoscale species of both low and high refractive index contrasts is possible. Our model accounts for a number of factors such as increased Brownian motion for particles with dimensions below 100 nm. Our results also highlight potential system changes such as slot width or particle refractive index that can be used to alter the expected trapping stability and transport speeds.

REFERENCES

- [1] D. Psaltis, S. R. Quake, and C. H. Yang, "Developing optofluidic technology through the fusion of microfluidics and optics," *Nature*, **442**, 381-386, (2006).
- [2] C. Monat, P. Domachuk, and B. J. Eggleton, "Integrated optofluidics: A new river of light," *Nature Photonics*, **1**, 106-114, (2007).
- [3] B. E. A. Saleh and M. C. Teich, *Fundamentals of photonics*. New York: Wiley, 1991.
- [4] P. Measor, S. Kuehn, E. J. Lunt, B. S. Phillips, A. R. Hawkins, and H. Schmidt, "Hollow-core waveguide characterization by optically induced particle transport," *Optics Letters*, **33**, 672-674, (2008).
- [5] X. L. Mao, J. R. Waldeisen, B. K. Juluri, and T. J. Huang, "Hydrodynamically tunable optofluidic cylindrical microlens," *Lab on a Chip*, **7**, 1303-1308, (2007).
- [6] P. Y. Chiou, A. T. Ohta, and M. C. Wu, "Massively parallel manipulation of single cells and microparticles using optical images," *Nature*, **436**, 370-372, (2005).
- [7] G. L. Liu, J. Kim, Y. Lu, and L. P. Lee, "Optofluidic control using photothermal nanoparticles," *Nature Materials*, **5**, 27-32, (2006).
- [8] R. W. Applegate, J. Squier, T. Vestad, J. Oakey, D. W. M. Marr, P. Bado, M. A. Dugan, and A. A. Said, "Microfluidic sorting system based on optical waveguide integration and diode laser bar trapping," *Lab on a Chip*, **6**, 422-426, (2006).
- [9] K. Grujic, O. G. Helleso, J. P. Hole, and J. S. Wilkinson, "Sorting of polystyrene microspheres using a Y-branched optical waveguide," *Optics Express*, **13**, 1-7, (2005).
- [10] R. F. Marchington, M. Mazilu, S. Kuriakose, V. Garcés-Chávez, P. J. Reece, T. F. Krauss, M. Gu, and K. Dholakia, "Optical deflection and sorting of microparticles in a near-field optical geometry," *Opt. Express*, **16**, 3712-3726, (2008).
- [11] A. Ashkin, "Acceleration and Trapping of Particles by Radiation Pressure," *Physical Review Letters*, **24**, 156-&, (1970).

- [12] A. Ashkin, J. M. Dziedzic, J. E. Bjorkholm, and S. Chu, "Observation of a Single-Beam Gradient Force Optical Trap for Dielectric Particles," *Optics Letters*, **11**, 288-290, (1986).
- [13] P. H. Jones, E. Stride, and N. Saffari, "Trapping and manipulation of microscopic bubbles with a scanning optical tweezer," *Applied Physics Letters*, **89**, 081113, (2006).
- [14] A. Ashkin and J. M. Dziedzic, "Optical Trapping and Manipulation of Viruses and Bacteria," *Science*, **235**, 1517-1520, (1987).
- [15] L. Bosanac, T. Aabo, P. M. Bendix, and L. B. Oddershede, "Efficient optical trapping and visualization of silver nanoparticles," *Nano Letters*, **8**, 1486-1491, (2008).
- [16] C. R. Pollock and M. Lipson, *Integrated photonics*. Boston ; London: Kluwer Academic, 2003.
- [17] S. Gaugiran, S. Getin, J. M. Fedeli, G. Colas, A. Fuchs, F. Chatelain, and J. Derouard, "Optical manipulation of microparticles and cells on silicon nitride waveguides," *Optics Express*, **13**, 6956-6963, (2005).
- [18] L. N. Ng, B. J. Luff, M. N. Zervas, and J. S. Wilkinson, "Propulsion of gold nanoparticles on optical waveguides," *Optics Communications*, **208**, 117-124, (2002).
- [19] B. S. Schmidt, A. H. Yang, D. Erickson, and M. Lipson, "Optofluidic trapping and transport on solid core waveguides within a microfluidic device," *Opt. Express*, **15**, 14322-14334, (2007).
- [20] A. H. J. Yang and D. Erickson, "Stability analysis of optofluidic transport on solid-core waveguiding structures," *Nanotechnology*, **19**, 045704, (2008).
- [21] D. B. Wolfe, R. S. Conroy, P. Garstecki, B. T. Mayers, M. A. Fischbach, K. E. Paul, M. Prentiss, and G. M. Whitesides, "Dynamic control of liquid-core/liquid-cladding optical waveguides," *Proceedings of the National Academy of Sciences of the United States of America*, **101**, 12434-12438, (2004).
- [22] A. H. J. Yang, S. D. Moore, B. S. Schmidt, M. Klug, M. Lipson, and D. Erickson, "Optical manipulation of nanoparticles and biomolecules in sub-wavelength slot waveguides," *Nature*, **457**, 71-75, (2009).

- [23] L. I. McCann, M. Dykman, and B. Golding, "Thermally activated transitions in a bistable three-dimensional optical trap," *Nature*, **402**, 785-787, (1999).
- [24] K. Kolasinski, *Surface Science: Foundations of Catalysis and Nanoscience*. West Sussex, England: John Wiley & Sons Ltd, 2002.
- [25] K. Svoboda and S. M. Block, "Biological Applications of Optical Forces," *Annual Review of Biophysics and Biomolecular Structure*, **23**, 247-285, (1994).
- [26] A. M. Armani and K. J. Vahala, "Heavy water detection using ultra-high-Q microcavities," *Optics Letters*, **31**, 1896-1898, (2006).
- [27] S. Gaugiran, S. Gétin, J. M. Fedeli, and J. Derouard, "Polarization and particle size dependence of radiative forces on small metallic particles in evanescent optical fields. Evidences for either repulsive or attractive gradient forces," *Opt. Express*, **15**, 8146-8156, (2007).
- [28] A. N. Grigorenko, N. W. Roberts, M. R. Dickinson, and Y. Zhang, "Nanometric optical tweezers based on nanostructured substrates," *Nature Photonics*, **2**, 365-370, (2008).
- [29] P. M. Hansen, V. K. Bhatia, N. Harrit, and L. Oddershede, "Expanding the optical trapping range of gold nanoparticles," *Nano Letters*, **5**, 1937-1942, (2005).

4.0 Optofluidic Ring Resonator Switch for Optical Particle Transport*

In this work, we demonstrate an optofluidic switch using a microring resonator architecture to direct particles trapped in the evanescent field of a solid-core waveguide. When excited at the resonant wavelength, light inserted into the bus waveguide becomes amplified within the ring structure. The resulting high optical intensities in the evanescent field of the ring generate a gradient force that diverts particles trapped on the bus to the ring portion of the device. We show that this increase in optical energy translates to an increase of 250% in the radiation pressure induced steady-state velocity of particles trapped on the ring. We also characterize the switching fraction of the device, showing that 80% of particles are diverted onto the ring when the device is at an on-resonance state. The optofluidic switch we present here demonstrates the versatility in exploiting planar optical devices for integrated particle manipulation applications.

4.1 Introduction

The fundamental principle behind the development of the lab-on-a-chip is to integrate numerous functions on a single device with the goal of reducing costs and increasing functionality. In recent years, much advancement has been made to integrate optical elements in the form of lenses [1-3], lasers [4, 5], waveguides [6, 7], and sensors [8, 9] with microfluidic devices. This research has coalesced into a field often referred to as optofluidics.

* This chapter was previously published in A. H. J. Yang and D. Erickson, "Optofluidic ring resonator switch for optical particle transport," *Lab on a Chip*, **10**, 769-774, (2010). Reproduced with permission from the Royal Society of Chemistry

Because of their flexibility and biocompatibility, free space optical tweezers have proven to be a useful tool for deflecting, sorting and transporting microparticles within lab-on-chip devices [10, 11]. Recently, researchers have demonstrated the ability to increase optical trapping forces on particles by using the evanescent field of planar waveguides [12-17]. To further augment the optical forces exerted on particles, other researchers have exploited devices like slotted waveguides [18] and plasmonic [19] structures to generate high-intensity field gradients for the trapping of nanoparticles and biomolecules with diameters as small as 50 nm. While this is highly advantageous for nanoscale trapping applications, they are limited for microparticle trapping and propulsion because the length scale that a nanophotonic trap can act over is much smaller. Another method by which the optical forces on microparticles can be increased is through the use of hollow-core [20, 21] and liquid-core/liquid-cladding waveguides [22] which enable the particle to directly interact with the optical mode rather than just the evanescent field.

Alternatively, one can achieve high optical intensities in planar waveguiding devices by incorporating a resonant structure, such as a whispering gallery mode (WGM) resonator. These resonators siphon a portion of light from a waveguide and recirculates the optical energy repeatedly along a circular path [23]. Resonance occurs when incoming light is in phase with light in a resonator that has completed a revolution around the structure. At specific discrete wavelengths, light will constructively interfere, resulting in a stronger optical intensity confined in the resonant structure relative to the bus waveguide [24]. This strong coupling correlates with a sharp drop in the bus waveguide output. This behavior associated with resonant structures enables WGM resonators to be used as nanoscale chemical [25] or biochemical [26] sensors. The large field amplification also applies to the evanescent

field of WGM devices. A recent paper by Arnold *et al.* [27] demonstrated the trapping and propulsion of 280 nm diameter nanoparticles on a spherical WGM resonator

Here we demonstrate, for the first time, an integrated microring resonator switch for optically trapped microparticles. As seen in Figure 4.1, our device consists of a microring resonator fabricated in SU-8 epoxy negative photoresist evanescently coupled to a bus waveguide of the same material. The path of trapped particles on the device is controlled by optical resonance and local field amplification in the ring creating an optical gradient force that pulls particles from the bus to the ring resonator. As we will demonstrate below, we can dynamically control the switch in real-time by changing the wavelength of the light at the input of the bus waveguide. To characterize the proposed mechanism for our switch, we determine the enhancement in propulsion velocity of particles trapped on the ring due to optical resonance. We also determine the overall efficiency of the ring resonator switch by measuring the fraction of particles routed onto the ring, which provides the optimal wavelengths for binary switch operation. Furthermore, we also describe our fabrication technique using controlled overexposure photolithography which enables ring structures with gap widths much smaller than the resolution of photolithography techniques, achieving controllable gap widths on the order of 100 nm in size.

4.2 Results and Discussion

Here, we describe the operating principle of the optofluidic ring resonator switch. Shown schematically in Figure 4.1, a continuous wave laser amplified by an erbium doped fiber amplifier (EDFA) is coupled into the bus waveguide. Some of the

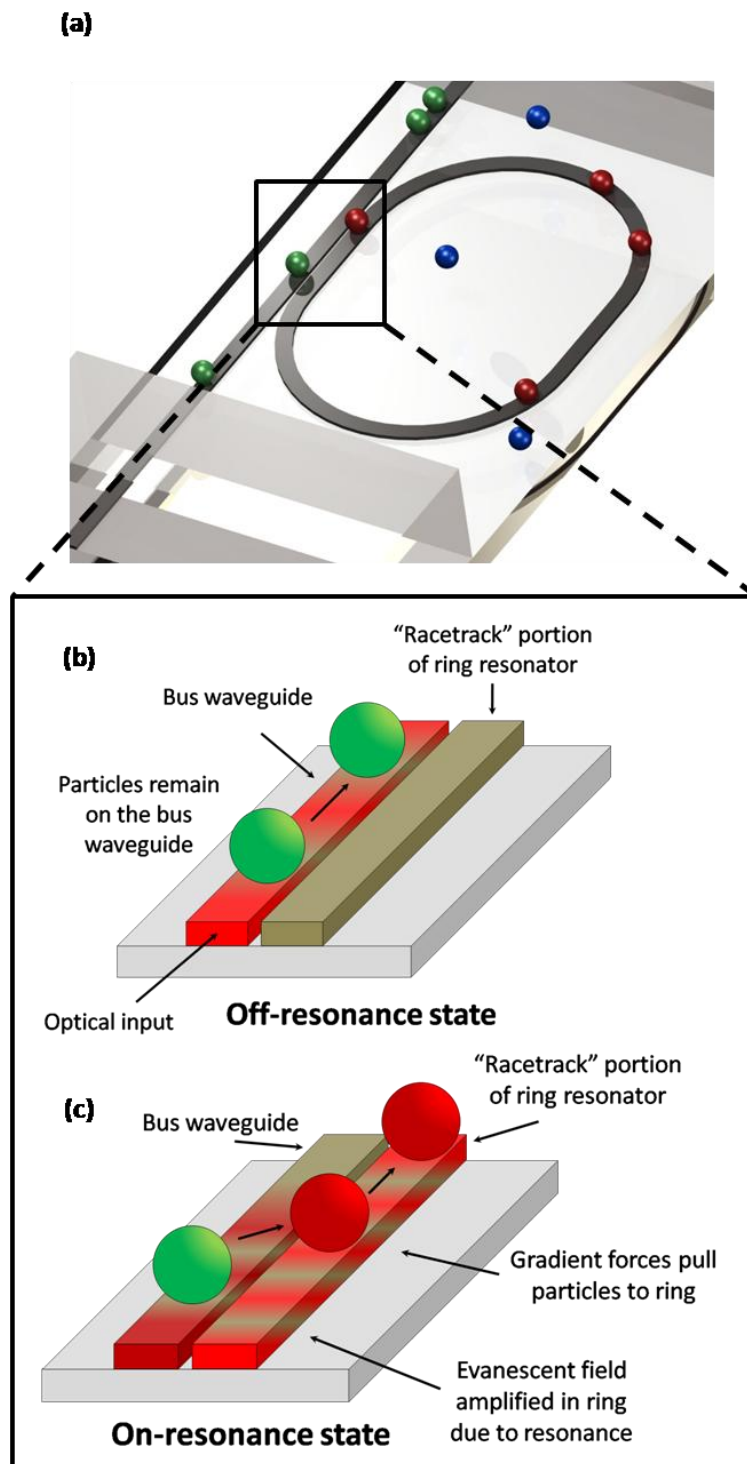


Figure 4.1: Schematic of optofluidic ring resonator switch. (a) Rendered picture of device with PDMS microfluidics. (b)-(c) Illustration of switching mechanism due to optical gradient forces when the ring strongly coupled at the resonant wavelength.

radiation extends into the ring waveguide in the region where the distance between bus and ring is smallest due to degenerate mode coupling. When the light that has traveled around the ring is in phase with incoming radiation, the waves constructively interfere resulting in a stronger optical field. The point at which light is most confined within the ring, known as the resonant wavelength, also results in a dramatic increase in the optical field confined within the ring. These resonating wavelengths of the structure are identified by a corresponding drop in the power output of the bus waveguide. The optical microring resonator switch operates by alternating between an on-resonance and off-resonance wavelength (about 1 nm). While the ring is on-resonance, particles trapped on the bus waveguide will be routed on the ring due to gradient forces arising from stronger local field intensities in the ring. In an off-resonance state, the bus waveguide will have a stronger relative intensity and the particles will tend to remain on the bus waveguide. To summarize, we exploit optical resonance in the ring and use wavelength of light to actively control the local optical field in our device and thus exert control over the path taken by optically trapped particles.

4.2.1 Particle switching using microring resonators

In Figure 4.2, we show a series of images that illustrate the active trapping and switching of 3 μm polystyrene microparticles by changing the wavelength of coupled light. Using light from a tapered lens fiber, the waveguides are excited at a wavelength near 1550 nm with an input power of 300 mW. To achieve particle switching, the wavelength of light is tuned from $\lambda_r = 1552.225$ nm, the resonant wavelength which exhibits the strongest drop in power at the end of the bus waveguide, to non-resonant wavelength, $\lambda_n = 1553.225$ nm. At λ_r , the majority of particles is trapped on the bus waveguide initially and is diverted onto ring due to

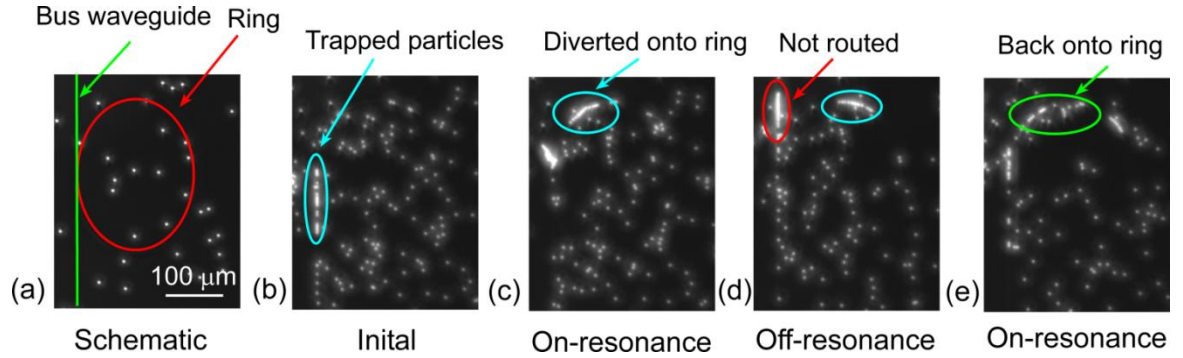


Figure 4.2: Active optical switching of particles on a microring resonator. This image sequence illustrates the switching effect by moving through an on-off-on resonance sequence. Here λ_r represents the resonant wavelength and λ_n represents the non-resonant wavelength. (a) Schematic of ring and bus waveguide overlay with CCD camera image. The same crop is used for all subsequent images. The dots represent 3 μm fluorescent polystyrene spheres. (b) Initial state of the system with a ‘string’ of particles trapped on the bus waveguide. (c) The trapped particles are diverted and continue to move forward on the ring. At this point, the input wavelength is changed to λ_n . (d) The next series of trapped particles pass through the switching junction and remain on the bus waveguide. The input wavelength is changed to λ_n . (e) Sequential particles are switched onto the ring structure again.

strong resonant coupling. After a series of particles have been diverted, the wavelength is changed 1 nm to λ_n , and the following set of particles to approach the switching junction bypass the ring and remain on the bus waveguide. We observe that particles that have been trapped on the ring while on-resonance will remain trapped and still be propelled when the ring is switched to an off-resonance state. Finally, after switching back to the resonant wavelength λ_r , the next series of trapped microparticles are diverted onto the ring structure.

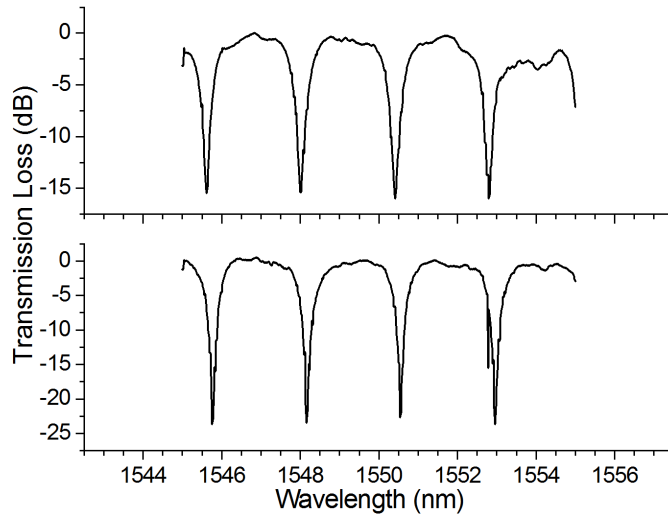
Qualitatively, during our experiments we have observed the premature release of particles on the bus waveguide before being routed onto the ring or propelled beyond the switching point. Similarly, we have observed that when multiple closely spaced particles arrive at the junction point, the particles will drift back and forth, creating a wave-like motion in the chain of particles. This could arise if the optical gradient

forces originating from both the bus waveguide and the resonator acting upon the particles simultaneously with the same relative magnitude of force and particles are not completely pulled over to the ring waveguide. A stronger optical resonance effect, represented by a higher quality factor (Q-factor), should lead to sharper differences in the optical intensity in the bus and ring waveguides at on-resonance wavelengths. Another potential explanation for this effect could be mode profile mismatch or bending losses due to the curvature of the ring resonator near the point where the wave-like motion of particles occurs. A future experiment to characterize this effect could examine particle switching between two evanescently coupled linear waveguides or a ring with an even large radius of curvature than the one described here.

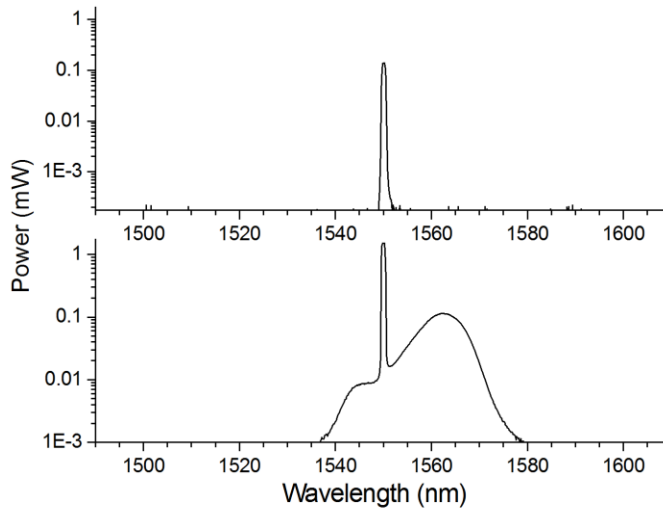
4.3 Device Characterization

It is well known that the radiation pressure force scales proportionally to the optical intensity. Therefore, we can infer the strength of the optical field in the ring by measuring the steady-state velocity of particles of trapped particles due to radiation pressure as a function of wavelength. Also, we can determine the switching efficiency, defined as the fraction of particles routed onto the ring to the number of total trapped particles at any given wavelength, by using particle tracking software to determine the total number of trapped particles and the number of particles routed onto the ring.

Our characterization of the particle transport and switching analyzes data obtained from two adjacent ring resonators with the same ring length on a single fabricated device. We define here ring A as the device that has a 296 nm gap width and ring B as the device with a 335 nm gap width. Both sets of results are used to illustrate how the degree of coupling enhances the velocity increase and switching of optically trapped



(a)



(b)

Figure 4.3: Optical transmission spectra of ring resonators and laser output. (a) The top spectra (ring A) represents a bus/ring gap width 30 nm smaller than the bottom (ring B). The rightmost resonance (~ 1552 nm) in both spectra is the one used in the EDFA amplified trapping and switching experiments. (b) The spectra of the unamplified light coming from a (top) 1550 tunable source and (bottom) after amplification using an EDFA. The output powers were plotted using a logarithmic scale.

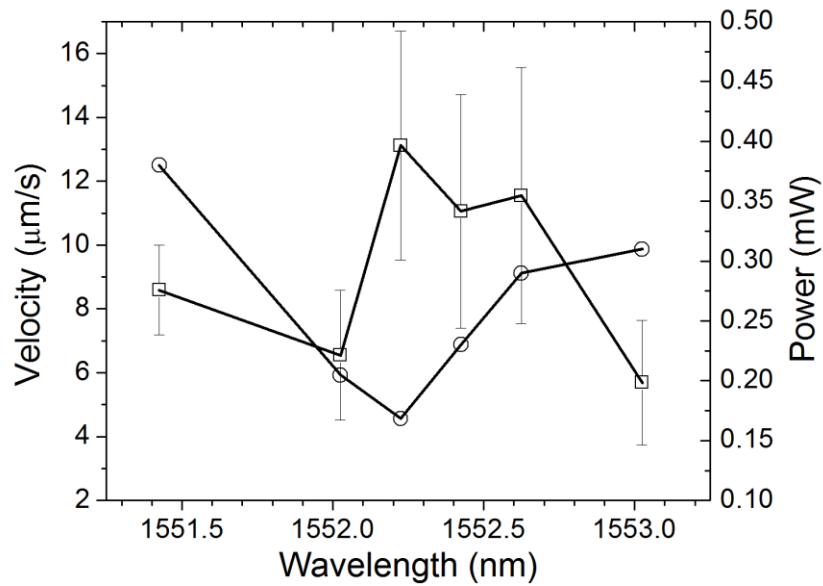
particles. Figure 3a shows the transmission spectra of the two adjacent ring resonator devices clad in water while excited by a 1550 nm tunable source. A 30 nm difference in the gap width of the two waveguides leads to a 10 dB difference in the power drop at the resonant wavelength. The quality factors of both rings, defined as $\lambda/\Delta\lambda$ at full width half maximum, are approximately 1550. The free spectral range of the devices is approximately 2 nm. As demonstrated previously by Levy *et al.* [28], changing the refractive index of the cover medium by flowing different media through the microfluidic channel can tune the coupling between the ring and bus waveguides resulting in a higher Q-factor. A more advanced device structure could incorporate a method to tune resonant wavelength of a microring structure, either via the electro-optic effect or microfluidic tuning [28].

Figure 4.3b illustrates the increase in broadband noise in the EDFA amplified light due to amplified spontaneous emissions. The spectra of light coming out of the 1550 nm tunable laser w/wo EDFA amplification were obtained using an optical spectrum analyzer. These emissions lead to a 100-fold increase in noise emissions in the 1530-1580 nm range. The increased noise and low free spectral range of our devices ensures a non-zero amount of light is always coupled into the ring resonator. This is likely the reason why particles can remain trapped and experience radiation pressure when the input wavelength can be considered off-resonance. If a strong optical resonance is required, as in the case for sensing applications involving the detection of small changes in the resonant wavelength due to binding events, then a notch filter can be used to filter out the non-excitation wavelengths.

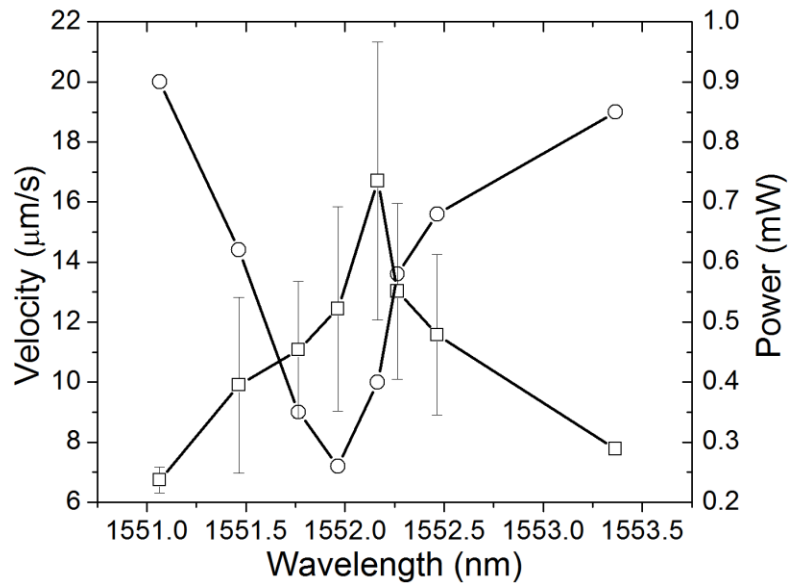
Figure 4.4 shows the measured steady-state velocity of 3 μm polystyrene beads on the ring portion of the resonator device as a function of optical wavelength and detected power at the output of the waveguides for two adjacent resonator devices. The velocity

enhancement for ring A was 200% and 250% for ring B defined here as the ratio of the average propulsion velocity of the particle during optical resonance vs its non-resonant propulsion velocity. As a control, we can compare the velocity increase for particles trapped on the ring to the velocity of particles trapped on the bus waveguide before the ring as a function of wavelength. The difference between the highest and lowest velocities measured on the bus waveguide was 24% and 36% for ring A and ring B respectively. As expected, the particles trapped on the bus waveguide do not experience the same velocity enhancement as particles trapped on the ring. The error bars in Figure 4.4 represent mechanical vibrations in the coupling fiber and changes in fluid velocity in the experimental system. We do acknowledge that this does lead to repeatability issues between different chips because losses in waveguides and differences in coupling can result in the same value for output power at the end of a waveguide while differing in the amount of actual coupled optical power. However, the observed trend of a velocity increase at optical resonance is observable across different experimental devices, even if the actual values of propulsion velocity cannot be easily correlated. The amount of noise can be reduced by using lenses to obtain better mode matching in the case of end-fire coupling or by using a different coupling mechanism such as a grating coupler [29].

The power drops measured for ring A and ring B at the resonant state are -3.5 db and -5.4 db respectively. We note that the increase in velocity for ring A is less pronounced in ring B due to the difference in gap width and most likely ring A is more weakly coupled than ring B. The drops in transmission when the ring is coupled are less steep in Figure 4.4 compared to Figure 4.3 due to the EDFA noise as described above. We observe that as the optical wavelength approaches the resonant wavelength of the ring resonator, output power in the bus waveguide decreases as resonator coupling



(a)

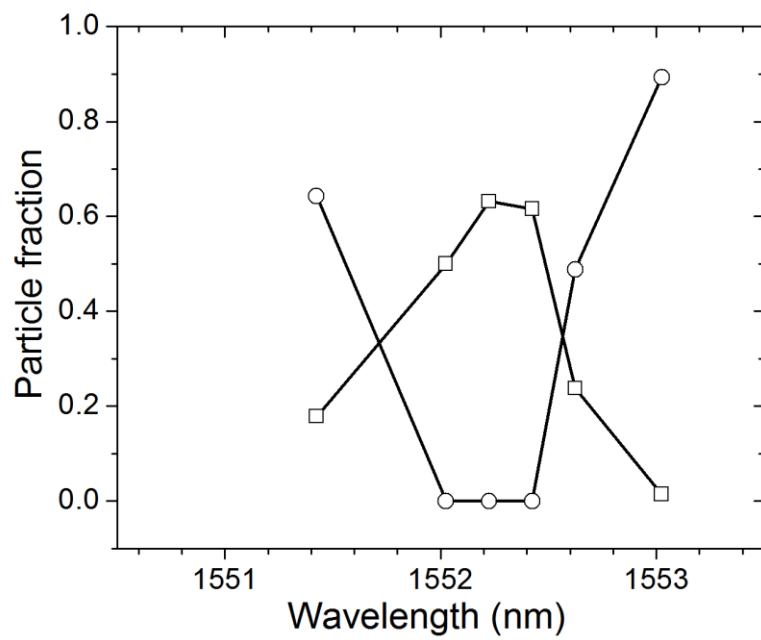


(b)

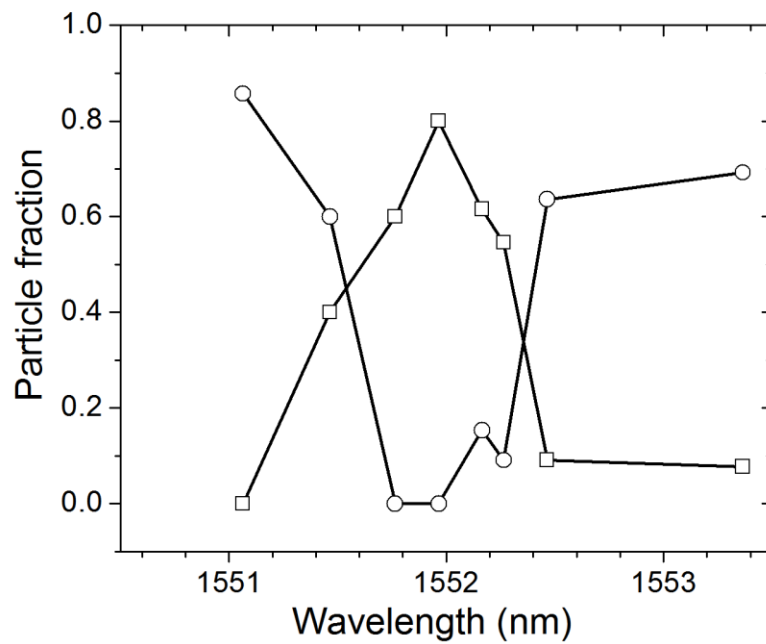
Figure 4.4: Enhancement of propulsion velocity. Plot of steady state velocity (squares) of 3 μm polystyrene beads trapped on rings and power output (circles) of the bus waveguide as a function of wavelength for (a) ring A and (b) ring B. Error bars for the velocity measurements are the standard deviation of velocity measurements due to fluctuation in guided power from mechanical vibration of the tapered lensed fiber used for coupling in the waveguide.

increases. This then leads to an increase in the propulsion velocity of trapped particles. Conversely, when the wavelength is off-resonance, the measured velocity is reduced from its on-resonance value. As stated previously, we determine the effectiveness of the resonator switch by directly measuring the fraction of particles routed onto the ring from the bus waveguide as a function of the input wavelength, as seen in Figure 4.5. We define the switch fraction as the number of particles that were successfully routed onto the ring over the total number of particles trapped initially on the bus waveguide. Similarly, we define the rejection fraction as the number of particles that remained on the bus waveguide without being routed onto the ring. For ring B, we can achieve an 80% switching fraction at the resonant wavelength, and an 80% rejection fraction when the ring is excited at a non-resonant wavelength. The switching fraction is lower for ring A; about 60% of the particles are diverted when the ring is on-resonance, due to weaker ring coupling. We expect that since the power drop measured from ring A is lower than ring B, that the amount of light coupled into the ring is smaller as well. This leads to a smaller net force experienced by the particle, and a smaller likelihood of pulling the particle over from the bus waveguide.

Figure 4.5: Particle switch efficiency as a function of input wavelength. (a) Fraction of particles that were routed onto the ring (squares) or bus waveguide (circles) plotted as a function of input wavelength for ring A and (b) ring B. We define particle fraction as a general term to represent the switching fraction (squares) of routed particles and the rejection fraction (circles) of particles that remained on the bus waveguide. The fractions shown here are calculated including particles that released at the switching junction due to trapping instability. The output power detected at the end of the bus waveguide (not shown here) is the same as in Figure 4.



(a)



(b)

4.4 Materials and methods

The SU-8 ring resonator devices were fabricated using stepper photolithography. The ring design was based on the racetrack design used previously by Levy *et al.* [28]. This design allows for a longer coupling distance compared to a completely circular ring structure. Our rings were 200 μm in diameter with a coupling length of 50 μm . The waveguide dimensions were designed to be 2 μm wide and 700 nm tall. The gap spacing between bus waveguide and resonator was specified to be 300 – 600 nm with a change in the gap distance of 30 nm between adjacent resonators. The ring gap after fabrication was often reduced by 200 – 300 nm due to controlled overexposure of the photoresist, creating much smaller gap features than normally possible using photolithography.

The photoresist was spun at 1000 RPM for 40 seconds on a fused silica substrate to achieve a film thickness of 700 nm. Exposure of the wafer was done using a i-line 5x stepper (GCA Autostep) at a computer controlled exposure time ranging from 0.20 – 0.3 seconds with an estimated intensity of 500 mW/cm^2 . The variability in exposure times shows the range of overexposure required for a sub-resolution gap between the bus waveguide and ring structure. Further optimization of the exposure time used an SEM analysis of dies at exposure intervals of 0.01 seconds. The waveguide devices were then diced and cleaved using a partial backside cleaving technique leaving a final edge width of 75-100 μm . This technique partially dices the device near the waveguide input and output and uses mechanical force to create a clean coupling edge for polymer on glass waveguiding devices.

The PDMS microchannels were made using standard fabrication techniques, using a microchannel master created from SU-8 2025 on a silicon wafer. The resulting

channels were 500 μm wide with a height of 25 μm and were bonded to the ring-resonator chip, leaving the input and output regions of the chip clad in air.

The light source used for exciting the waveguides is a 1550 nm tunable erbium-doped fiber laser which is further amplified using an EDFA to achieve the necessary powers for trapping. Light is coupled into the waveguides using a tapered lens fiber. Polarization of the light entering the waveguides was determined using a polarization filter and controller. All the experiments conducted here were done using transverse electric (TE) polarized waves. This was done to maintain consistency across the experiment and minimize differences in coupling and propagating losses. The waveguides have a 3 mm offset with a 500 μm bending radius. The optical losses in these waveguides were previously characterized by Schmidt *et al.* [17].

In our experimental system, we use a pressure-driven flow induced by a syringe pump to flow 3 μm diameter fluorescent polystyrene beads in the microchannels over the ring resonator device. The particles were suspended in a pH 7.0 buffer solution with 1% w/v Triton X-100 surfactant to mitigate particle adsorption on surfaces. When the bus waveguide is optically excited, the particles are trapped both on the bus waveguide and on the ring resonator structures. Trapped particles exhibit radiation pressure propulsion in the direction of optical propagation. We use a CCD camera (Hamamatsu C472-80) and Video Spot Tracker software to determine the steady state velocity of trapped particles. The switch efficiency were determined by analyzing the image stacks using the ImageJ software to determine the number of particles which were initially trapped on the bus waveguide that were diverted onto the ring structure.

4.5 Conclusions

In summary, we have demonstrated an optically driven microring resonator particle switch that is easily integrated with waveguide-based optofluidic transport architectures. The switch mechanism we present here uses the natural amplification of optical energy in the ring to divert trapped particles either onto the ring or along the bus depending on whether the excitation wavelength corresponds to a resonant or non-resonant condition. We show that we can achieve a 250% enhancement of the steady-state velocity of trapped particles along with an 80% switching fraction.

REFERENCES

- [1] X. L. Mao, S. C. S. Lin, M. I. Lapsley, J. J. Shi, B. K. Juluri, and T. J. Huang, "Tunable Liquid Gradient Refractive Index (L-GRIN) lens with two degrees of freedom," *Lab on a Chip*, **9**, 2050-2058, (2009).
- [2] X. L. Mao, J. R. Waldeisen, B. K. Juluri, and T. J. Huang, "Hydrodynamically tunable optofluidic cylindrical microlens," *Lab on a Chip*, **7**, 1303-1308, (2007).
- [3] S. K. Y. Tang, C. A. Stan, and G. M. Whitesides, "Dynamically reconfigurable liquid-core liquid-cladding lens in a microfluidic channel," *Lab on a Chip*, **8**, 395-401, (2008).
- [4] Z. Y. Li, Z. Y. Zhang, T. Emery, A. Scherer, and D. Psaltis, "Single mode optofluidic distributed feedback dye laser," *Optics Express*, **14**, 696-701, (2006).
- [5] D. Nilsson, S. Balslev, M. M. Gregersen, and A. Kristensen, "Microfabricated solid-state dye lasers based on a photodefinable polymer," *Applied Optics*, **44**, 4965-4971, (2005).
- [6] E. J. Lunt, P. Measor, B. S. Phillips, S. Kuhn, H. Schmidt, and A. R. Hawkins, "Improving solid to hollow core transmission for integrated ARROW waveguides," *Optics Express*, **16**, 20981-20986, (2008).
- [7] D. B. Wolfe, R. S. Conroy, P. Garstecki, B. T. Mayers, M. A. Fischbach, K. E. Paul, M. Prentiss, and G. M. Whitesides, "Dynamic control of liquid-core/liquid-cladding optical waveguides," *Proceedings of the National Academy of Sciences of the United States of America*, **101**, 12434-12438, (2004).
- [8] C. Y. Chao and L. J. Guo, "Biochemical sensors based on polymer microrings with sharp asymmetrical resonance," *Applied Physics Letters*, **83**, 1527-1529, (2003).
- [9] L. N. Jiang and S. Pau, "Integrated waveguide with a microfluidic channel in spiral geometry for spectroscopic applications," *Applied Physics Letters*, **90**, 111108, (2007).
- [10] R. W. Applegate, J. Squier, T. Vestad, J. Oakey, D. W. M. Marr, P. Bado, M. A. Dugan, and A. A. Said, "Microfluidic sorting system based on optical waveguide integration and diode laser bar trapping," *Lab on a Chip*, **6**, 422-426, (2006).
- [11] M. P. MacDonald, G. C. Spalding, and K. Dholakia, "Microfluidic sorting in an optical lattice," *Nature*, **426**, 421-424, (2003).

- [12] S. Gaugiran, S. Getin, J. M. Fedeli, and J. Derouard, "Polarization and particle size dependence of radiative forces on small metallic particles in evanescent optical fields. Evidences for either repulsive or attractive gradient forces," *Optics Express*, **15**, 8146-8156, (2007).
- [13] K. Grujic, O. G. Helleso, J. P. Hole, and J. S. Wilkinson, "Sorting of polystyrene microspheres using a Y-branched optical waveguide," *Optics Express*, **13**, 1-7, (2005).
- [14] J. P. Hole, J. S. Wilkinson, K. Grujic, and O. G. Helleso, "Velocity distribution of Gold nanoparticles trapped on an optical waveguide," *Optics Express*, **13**, 3896-3901, (2005).
- [15] H. Y. Jaising and O. G. Helleso, "Radiation forces on a Mie particle in the evanescent field of an optical waveguide," *Optics Communications*, **246**, 373-383, (2005).
- [16] L. N. Ng, B. J. Luff, M. N. Zervas, and J. S. Wilkinson, "Propulsion of gold nanoparticles on optical waveguides," *Optics Communications*, **208**, 117-124, (2002).
- [17] B. S. Schmidt, A. H. Yang, D. Erickson, and M. Lipson, "Optofluidic trapping and transport on solid core waveguides within a microfluidic device," *Opt. Express*, **15**, 14322-14334, (2007).
- [18] A. H. J. Yang, S. D. Moore, B. S. Schmidt, M. Klug, M. Lipson, and D. Erickson, "Optical manipulation of nanoparticles and biomolecules in sub-wavelength slot waveguides," *Nature*, **457**, 71-75, (2009).
- [19] A. N. Grigorenko, N. W. Roberts, M. R. Dickinson, and Y. Zhang, "Nanometric optical tweezers based on nanostructured substrates," *Nature Photonics*, **2**, 365-370, (2008).
- [20] P. Measor, S. Kuehn, E. J. Lunt, B. S. Phillips, A. R. Hawkins, and H. Schmidt, "Hollow-core waveguide characterization by optically induced particle transport," *Optics Letters*, **33**, 672-674, (2008).
- [21] P. Measor, L. Seballos, D. L. Yin, J. Z. Zhang, E. J. Lunt, A. R. Hawkins, and H. Schmidt, "On-chip surface-enhanced Raman scattering detection using integrated liquid-core waveguides," *Applied Physics Letters*, **90**, -, (2007).

- [22] S. K. Y. Tang, B. T. Mayers, D. V. Vezenov, and G. M. Whitesides, "Optical waveguiding using thermal gradients across homogeneous liquids in microfluidic channels," *Applied Physics Letters*, **88**, -, (2006).
- [23] F. Vollmer and S. Arnold, "Whispering-gallery-mode biosensing: label-free detection down to single molecules," *Nature Methods*, **5**, 591-596, (2008).
- [24] C. R. Pollock and M. Lipson, *Integrated photonics*. Boston ; London: Kluwer Academic, 2003.
- [25] A. M. Armani and K. J. Vahala, "Heavy water detection using ultra-high-Q microcavities," *Optics Letters*, **31**, 1896-1898, (2006).
- [26] I. M. White, H. Oveys, X. Fan, T. L. Smith, and J. Y. Zhang, "Integrated multiplexed biosensors based on liquid core optical ring resonators and antiresonant reflecting optical waveguides," *Applied Physics Letters*, **89**, 191106, (2006).
- [27] S. Arnold, D. Keng, S. I. Shopova, S. Holler, W. Zurawsky, and F. Vollmer, "Whispering gallery mode carousel - a photonic mechanism for enhanced nanoparticle detection in biosensing," *Optics Express*, **17**, 6230-6238, (2009).
- [28] U. Levy, K. Campbell, A. Groisman, S. Mookherjea, and Y. Fainman, "On-chip microfluidic tuning of an optical microring resonator," *Applied Physics Letters*, **88**, 111107, (2006).

5.0 Future work and conclusions

5.1 Future Work

This chapter describes an opportunity for future work in the development and study of optofluidic transport. To summarize, the main contribution of this work has been the design, demonstration, and characterization of integrated nanophotonic devices for optofluidic transport and control. More specifically, the ring resonators and slotted waveguides were used to trap and transport particles and large molecules suspended in the fluid medium rather than a fluid itself. This presents an interesting challenge since fluid manipulation through optical devices could enable entirely new methods for processing in microfluidic devices. This section will describe an experimental system that could be used to extend optofluidic transport to ‘fluid particles’ such as multi-phase liquid emulsions.

The primary optical forces at work for optofluidic manipulation depend largely on photon scattering and electromagnetic polarization phenomena and are therefore more suited towards small solid particles. While a suspension of particles in a fluid can describe many biological samples of interest such as blood or serum, this is often not true for a system that is a mixture of small molecules. In the case of a solution, the constituent molecules are small enough (atomic scale) that the fluid is described as a continuum phase rather than as a suspension of atomic particles. Recent work by Casner and Delville [1] demonstrated that an optical force can be exerted on a fluid-fluid interface. In this work, a beam was focused on the interface between two immiscible fluids and the interface was shown to deform due to the photon pressure. From this work, the hypothesis would be that if a fluid contained as a droplet within another immiscible phase would result in a fluid ‘particle’ that could be affected as a solid particle would. In this case, the emulsion bubble would be an enclosed region

with a different refractive index than the surrounding medium and can be affected by the same gradient and propulsion forces that would affect a solid particle.

Droplets are used in microfluidic systems in a number of different configurations. Digital microfluidics is a term used to describe an open device where discrete droplets rest on a dielectric substrate and are controlled through an applied electric field. The electric field alters the solid-liquid contact angle of the droplet and enables a controlled digital movement of the droplet on the dielectric surface. Electrowetting on dielectrics or EWOD has been used to develop devices capable of complex chemical processing using the movement and coalescence of the droplets for mixing and reaction operations. The other primary configuration is an enclosed system where the droplets are created from two immiscible phases under continuous flow within a microfluidic channel. Droplet breakup occurs as the shear forces at the interface between the two immiscible phases causes a droplet to be pinched off from the droplet forming stream. The geometry of the channel needed to generate monodisperse droplets can vary depending on the size of droplets required. Two commonly used channel configurations are T-junction channels [2] or cross-junction channels [3] with a pre-determined orifice for controlled droplet breakup. In these cases, the droplet stream often contains a hydrophilic medium such as water and the sheath streams contain a hydrophobic medium like mineral oil. It is important that the channels containing the droplet and sheath streams are relatively hydrophobic otherwise wetting on the surfaces of the channel will make droplet generation more difficult.

There are several advantages to developing a method for the optofluidic manipulation of liquid droplets. A liquid droplet could act as a larger vehicle that can carry solutions that are difficult to manipulate directly. This would enable the ability to work in systems where it would be not ideal to bind a sample to a solid surface such as for

studies of protein folding. It is well known that fluid interfaces can be used as optically smooth surfaces for making adaptable mirrors or reconfigurable lenses. Along those same lines, an emulsion droplet would have an optically smooth surface which could be exploited as an optical biosensor. One potential mechanism would be to use a waveguide as a source for exciting an optical resonance along the surface of the droplet. Previous work has shown that such resonances can be excited in large microspheres with diameters as small as 20 μm . An optically smooth droplet surface could enhance the resonance effect enabling low-mass sensitivity detection of chemicals contained within the droplet. There is also potential in developing applications for highly multiplexed sensing as each droplet is isolated or combining droplets to trigger a chemical reaction that can be monitored optically from a nearby waveguide.

Here I describe a potential experimental system that could be used in conjunction with optical waveguides for manipulating water-in-oil emulsion droplets. The fabrication described here is similar to the architecture described previously by Schmidt *et al.*, however, the procedures here have been optimized for use with droplet emulsions. SU-8 waveguides with a height of 600 nm and a width of 2.7 μm are patterned onto a fused silica substrate using stepper photolithography. The devices are formed by a backside dicing technique at the coupling points where the waveguide features are covered with S-1813 photoresist, cut partially using a dicing saw, and then cleaved along the cut lines. The chips can then be bonded with PDMS microchannels with a T-junction or cross-junction droplet generation geometry. The PDMS layer is formed from a mixture of a PDMS monomer and cross-linker which is mixed, allowed to sit for 30 – 45 minutes and then baked at 80 $^{\circ}\text{C}$ for about 1 hour. Afterwards, the input and output holes are punched and both substrate and PDMS are exposed to oxygen

plasma for 45 seconds to a minute. After the substrate and PDMS are bonded, the chips are baked again at 80 °C for about 18+ hours. This technique ensures strong PDMS-glass bonding and that the PDMS is hydrophobic after exposure to oxygen plasma.

In order to attract the droplet toward a waveguide, the refractive index of the droplet phase needs to be higher than the fluid medium. One possibility is in using a higher index fluid or modifying the refractive index of the droplet phase by dissolving a salt, such as calcium chloride, which will modify the index of the solution. If biocompatibility is a concern where a tightly regulated pH and saline environment is required, another possibility is in choosing an oil phase that has a lower refractive index than the droplet phase. Fluorinated oils such as those commercially developed by 3M (Fluorinert FC-72) have indexes of refraction $n = 1.25$ which would be lower than a buffered water solution. These oils have been successfully used by past researchers in creating water-in-oil droplet emulsions in microfluidics. However, because the index difference is smaller compared to a polystyrene bead in water ($n_{\text{diff}} = 0.08$ for the water-in-oil droplets compared to $n_{\text{diff}} = 0.26$ for polystyrene), a decrease in the optical forces that can be exerted should be expected as well.

While previous works have demonstrated the use of a fluorinated oil/water system [4] for droplet generation, there are additional challenges due to working in a heterogeneous liquid environment compared to the systems described in Chapters 2 – 4 previously. As droplet pinch-off is dependent upon both flow shear forces and the surface tension of the droplet interfaces, it is difficult to generate droplet sizes using a geometric droplet generation technique as those described above. In general, droplets created using this method range in diameter from 20 – 100 μm in diameter. There have been reports in the literature of techniques such as surfactant mediated tip-streaming

[5] which focuses on creating monodisperse secondary droplets from larger droplets which can create micron sized droplets. This can be important as a larger droplet size would experience much larger fluid drag forces which scales linearly with increasing particle size. This would inhibit any forward momentum generated by radiation pressure or gradient forces. Also, buoyancy forces become important as the droplets can often be filled with a fluid of different density than the medium. In the experiments described in Chapters 2 – 4, the particles are density matched to the solution such that buoyancy forces are minimized. In the case of the water/FC-72 system detailed here, the specific gravity of the oil phase is 1.7, much higher than a water phase droplet. This buoyancy effect creates an additional lift force that must also be considered and balanced against the optical gradient force and radiation pressure forces. The challenge for an all-liquid optofluidic transport system will be in choosing a fluid system that contains the right optical and hydrodynamic properties to allow for manipulation similar to solid polystyrene spheres. The advantages in this approach such as using a liquid droplet as a chemical carrier and as a vehicle for real-time optical monitoring would greatly increase the applications for droplet lab-on-a-chip technology.

5.2 Summary and Conclusion

In summary, this dissertation discusses a number of advancements in nanophotonic optofluidic transport for biomolecules and controlling particles. The devices are based on previous work by the author on the integration of PDMS microfluidics and waveguides for the manipulation of microparticles. Demonstrated for the first time here was the successful trapping and optical transport of polystyrene nanoparticles and DNA biomolecules suspended in active flow using the evanescent field of a slotted waveguide. Applications of this shown included the concentration of multiple particles

and the ability to measure the strength of the trap through a kinetic particle release analysis. A comprehensive analytical and numerical analysis was conducted to understand particle trapping stability within similar slot waveguide systems and to determine the practical limit of trapping for metallic and polystyrene nanoparticles. The results from the study will be of use to future researchers developing nanophotonic devices for nanoparticle or biomolecular manipulation. Extending upon methods for the control of trapped particles is the design and characterization of an optical switch using an SU-8 ring resonator. The immediate impact of this work will hopefully drive research into nanophotonic manipulation using a variety of different architectures, such as photonic crystals and plasmonic structures. There is a breadth of research in controlling light in many creative ways many mentioned in this dissertation. Exploiting these nanostructures can potentially pave the way for

The true impact of this work is in illustrating the potential of using all types of photonic devices for optical transport. Outlined briefly was a plan to use the microfluidic/waveguide architecture developed here for the transport of liquid water-oil droplets which would open an entire new class of optofluidic manipulation.

REFERENCES

- [1] A. Casner and J. P. Delville, "Laser-induced hydrodynamic instability of fluid interfaces," *Physical Review Letters*, **90**, -, (2003).
- [2] G. F. Christopher, N. N. Noharuddin, J. A. Taylor, and S. L. Anna, "Experimental observations of the squeezing-to-dripping transition in T-shaped microfluidic junctions," *Physical Review E*, **78**, -, (2008).
- [3] W. Lee, L. M. Walker, and S. L. Anna, "Role of geometry and fluid properties in droplet and thread formation processes in planar flow focusing," *Physics of Fluids*, **21**, -, (2009).
- [4] R. Tewhey, J. B. Warner, M. Nakano, B. Libby, M. Medkova, P. H. David, S. K. Kotsopoulos, M. L. Samuels, J. B. Hutchison, J. W. Larson, E. J. Topol, M. P. Weiner, O. Harismendy, J. Olson, D. R. Link, and K. A. Frazer, "Microdroplet-based PCR enrichment for large-scale targeted sequencing (vol 27, pg 1025, 2009)," *Nature Biotechnology*, **28**, 178-178, (2010).
- [5] S. L. Anna and H. C. Mayer, "Microscale tipstreaming in a microfluidic flow focusing device," *Physics of Fluids*, **18**, -, (2006).